Consistent Histories Formulation of the Double-Slit Experiment

by

Benjamin Noë Bauml

A THESIS

submitted to

Oregon State University

Honors College

in partial fulfillment of

the requirements for the

degree of

Honors Baccalaureate of Science in Physics and Mathematics

(Honors Scholar)

Presented 30 April 2020

Commencement June 2020

Abstract

Benjamin Noë Bauml for the degree of Honors Bachelor of Science in Physics and Mathematics, presented on 30 April 2020.

Title: Consistent Histories Formulation of the Double-Slit Experiment

Approved: _____

David A. Craig

The standard interpretation of quantum mechanics (known as the Copenhagen interpretation) divides the world into quantum phenomena and classical observers that perform measurements upon the phenomena. This provides a quite functional framework for calculating probabilities of measurement outcomes, but it lacks the generality necessary for such things as retrodiction, and examination of situations in which there cannot be classical observers.

Enter the consistent (or decoherent) histories formalism, which provides a consistent framework for assigning and interpreting quantum probabilities even in the absence of classical observers. In order to aid others in adopting the formalism, I herein examine the double-slit experiment within the framework of the consistent histories formalism.

For my first trick, I replicate the results of basic geometric optics applied to Young's experiment. Second, a detector model is included to make the interference pattern vanish, demonstrating the shift from wave behavior to particle behavior. Finally, certain approximations are removed to examine the case of non-infinitesimal slits. By not appealing to the outside world of observers, the consistent histories formalism is ideally suited for demonstrating the link between persistent records and the transition to the classical realm, crossing smoothly through paradoxical domains where a particle can diffract like a wave.

Key Words: consistent histories, decoherence, double-slit experiment, interference, path detection

Corresponding Email Address: baumlb@oregonstate.edu

30 April 2020

Consistent Histories Formulation of the Double-Slit Experiment

by

Benjamin Noë Bauml

A THESIS

submitted to

Oregon State University

Honors College

in partial fulfillment of

the requirements for the

degree of

Honors Baccalaureate of Science in Physics and Mathematics

(Honors Scholar)

Presented 30 April 2020

Commencement June 2020

Honors Bachelor of Science in Physics and Mathematics project of Benjamin Noë Bauml presented on 30 April 2020.

APPROVED:

David A. Craig, Mentor, representing Physics

Elizabeth Gire, Committee Member, representing Physics

Janet Tate, Committee Member, representing Physics

Toni Doolen, Dean, Oregon State University Honors College

I understand that my project will become part of the permanent collection of the Oregon State University Honors College. My signature below authorizes release of my project to any reader upon request.

Benjamin Noë Bauml, Author, representing without a law degree

Contents

Chapter 1

Background

1.1 What Came Before

The Copenhagen interpretation is the baseline formalism that underlies your average undergraduate coursework on quantum mechanics. For what it's worth, it does well enough for such purposes. Oftentimes, it is sufficient to consider the classical and quantum realms as discrete. Without ever needing to go beyond this dichotomy, we can consider all kinds of quantum phenomena, from quantized spins, to scattering problems, to hydrogen orbitals, and beyond. When the outside world wants to take a peek, a "measurement" occurs, and we calculate the probabilities of the possible outcomes [1]. However, like Barad-dûr, this split premise can come crashing down, not at the melting of the One Ring, but in the face of a simple question: How do we make predictions without classical observers [2]?

Perhaps you scoff at this question at first. After all, if something cannot be observed and studied, even indirectly, what possible relevance could it have? I ask you to ruminate on the early universe, before humans, before revolving planets, before existence governed by classical mechanics. All of the classical physics we know and love is an emergent phenomenon, and some rules must exist governing how it coalesced out of quantum mechanics. We need a framework, applicable even to closed systems, which enables us to make predictions and assign probabilities. One approach is the consistent histories formalism[1] [4].

The foundation of the formalism stems initially from the work of Hugh Everett, who proposed a generalization of the Copenhagen interpretation to closed systems in 1957 [5]. This was extended further by Murray Gell-Man and James Hartle [6, 7], whose endeavors paralleled and built upon the independent work of Robert Griffiths [8] and Roland Omnés [9], as well as Zeh, Zurek, and Joos [10, 11, 12].

Learning a new formalism can be challenging; even if the how-to of it is explained, there is just something lacking if one cannot see the method in action. My purpose here is to provide such an example, applying the

[1] Another interesting approach involving nonlocal hidden variables is Bohmian quantum mechanics, in which particles are classical, but acted upon by a quantum potential determined by the entire system. A general overview of David Bohm's interpretation can be found in [3].

consistent histories formalism to a foundational quantum mechanics experiment. Effectively, I am attempting to construct a pedagogical aid for those wishing to follow in the footsteps of us Consistenturions.[2]

The which if you with patient ears attend,
What here shall miss, our toil shall strive to mend.

—final couplet of the opening sonnet of *Romeo and Juliet*

1.2 The Double Slit Experiment

'Why the double-slit experiment?' I pretend to hear you ask. The double-slit experiment (depicted in Fig. 1.1) was first performed by Thomas Young in 1801 to demonstrate the wave nature of light [13]. A screen pierced by two slits is set up in front of a second screen, called the detecting screen, and light is allowed to impinge upon the slits. When the light diffracts on the other side of the slits, the expanding pair of waves overlap and interfere. As a result, bright fringes from constructive interference and dark bands from destructive interference appear on the detecting screen.

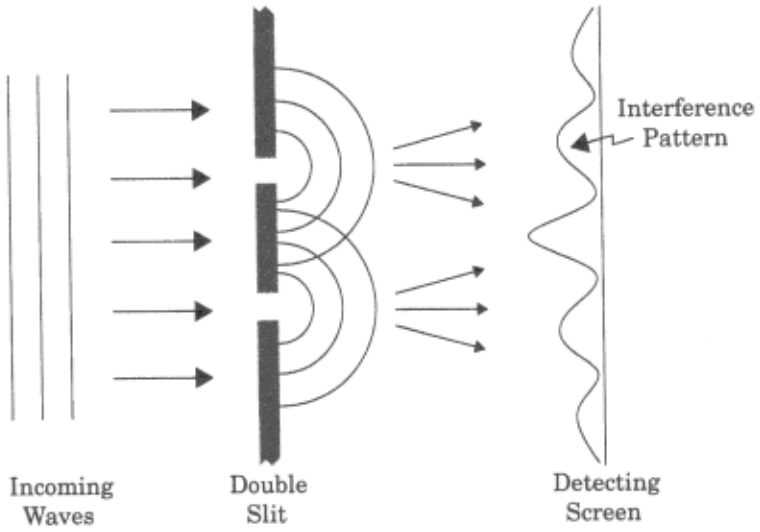

Figure 1.1: Young's Experiment This is Figure 1-11 from *The Quantum Challenge* [3]. The light waves approach from the left, then diffract beyond the pair of slits. As waves overlap, they interfere, causing a pattern of bright and dark bands to appear on the detecting screen.

As fascinating as this result is, the double-slit experiment has evolved. In 1989, Akira Tonomura and his colleagues tested the idea of matter waves [14], first conceived by Louis de Broglie in 1942. To do this, they constructed an apparatus which shot electrons between a pair of grounded plates, around a positively charged wire. Actual slits were not involved, but the device, seen in Fig. 1.2, affected the electrons in the same manner. The electrons were introduced to the device at such a low rate that only one electron was

[2] I completely made this name up, but I hope it catches on.

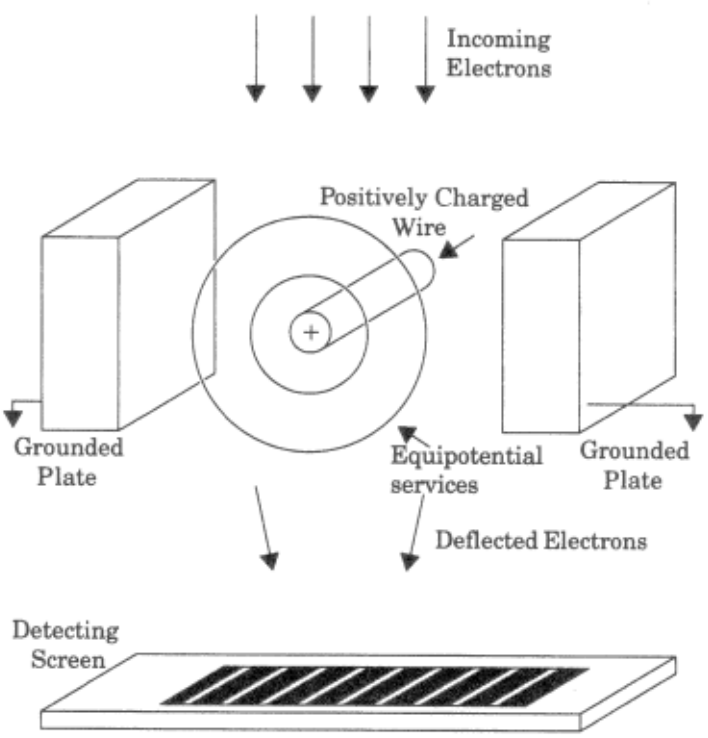

Figure 1.2: The Experiment of Tonomura et al. This is Figure 1-1 from *The Quantum Challenge* [3], modified from the source [14]. Electrons are shot one at a time through the gap between two grounded plates, which is bisected by a positively charged wire. The electrons are deflected in transit, then have their end positions recorded by striking a detecting screen. Though not truly a double-slit, the device replicates the same geometry in its action upon the electrons.

within the device at a time, removing the possibility of confounding effects arising from interactions between electrons. The astounding result (visible in the left column of Fig. 1.3) was that a pattern of light and dark bands was built up particle by particle, indicating that each electron interfered with itself in transit, acting in a manner consistent with wave behavior.

The matter wave result of the double-slit experiment can be approached from a wave optics perspective [1, 3]. Say you have a particle with momentum p passing through a double-slit apparatus. The plane wave $Ae^{ipr_u/\hbar}$ represents the wave function exiting the upper slit, while the plane wave $Ae^{ipr_l/\hbar}$ represents the wave function exiting the lower slit. As depicted in Fig. 1.4, the values r_u and r_l are distances from the upper and lower slits, respectively, to a particular point on the screen, thus making them functions of y. The wave function at the screen created by both slits would be

$$\psi(y) = A(e^{ipr_u/\hbar} + e^{ipr_l/\hbar}). \tag{1.1}$$

This can be restated more simply by recalling that the deBroglie wavelength is $\lambda_{dB} = h/p = 2\pi\hbar/p$:

$$\psi(y) = A(e^{i2\pi r_u/\lambda_{dB}} + e^{i2\pi r_l/\lambda_{dB}}). \tag{1.2}$$

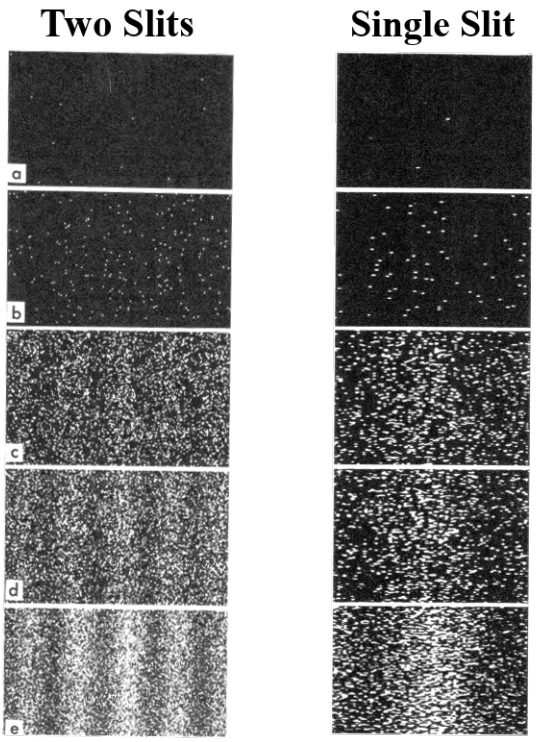

Figure 1.3: Two Experiments: Both Slits Open Versus One Slit Open The two columns of images are Figure 1-3 (on left) and Figure 1-4 (on right) from *The Quantum Challenge* [3], taken originally from [14]. Ten electrons had arrived in panel (a), 100 in panel (b), 3000 in panel (c), 20,000 in panel (d), and 70,000 in panel (e). Though we consider electrons to be particles, and they passed through the device one at a time, an interference pattern emerged on the detecting screen. In contrast, closing one of the slits caused the interference pattern to vanish, and the electrons just build up beyond the slit like a normal volley of particles.

To get the interference pattern, one must find the probability density by squaring the wave function:

$$\begin{aligned}
\mathscr{P}(y) &= |\psi(y)|^2 \\
&= |A(e^{i2\pi r_u/\lambda_{dB}} + e^{i2\pi r_l/\lambda_{dB}})|^2 \\
&= |A|^2 \left(e^{i2\pi r_u/\lambda_{dB}} + e^{i2\pi r_l/\lambda_{dB}}\right)\left(e^{-i2\pi r_u/\lambda_{dB}} + e^{-i2\pi r_l/\lambda_{dB}}\right) \\
&= |A|^2 \left(2 + e^{i2\pi (r_u - r_l)/\lambda_{dB}} + e^{-i2\pi (r_u - r_l)/\lambda_{dB}}\right) \\
&= 2|A|^2 \left(1 + \cos\left(2\pi \frac{r_u - r_l}{\lambda_{dB}}\right)\right).
\end{aligned} \tag{1.3}$$

This oscillatory formula describes the interference pattern. Note that it is not normalized, so further analysis would be required to provide calculable probabilities. The general shape is still useful, however.

It is important to note that interference only crops up when one considers events *in sequence*. If we looked at the possible values a single observable could take, the outcomes could not possibly interfere with each other.[3] In the experiments of Young and Tonomura et al, the incoming waves or particles first encounter

[3]See Section 2.3, particularly the discussion leading to Eqn. 2.17 and the conclusion that the final element of a history always decoheres from the alternatives.

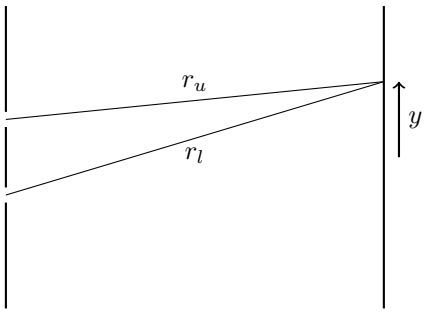

Figure 1.4: Double-Slit Experiment Simplified Apparatus Waves exit the upper and lower slits and travel to a field point at height y on the detector screen. Waves exiting the upper slit cover distance r_u, while waves exiting the lower slit cover distance r_l. The path length difference generates interference fringes.

the slits, then the detector screen. The path through the upper slit to the field point at the detector screen interferes with the path through the lower slit terminating at the same location.[4] As you shall see, time-sequenced events are the bread and butter of the consistent histories formalism.

Aside from that, we must also acknowledge that the double-slit experiment is truly two experiments. With both slits open, one gets interference as in Young's experiment, but closing one slit or employing a path detector to distinguish which slit a quanton goes through creates an entirely different situation. In stark contrast, the second experiment leads to particle-like behavior[5] (see the right column of Fig. 1.3), and a particle that is also a wave constitutes a classical incompatibility. With the persistent forward march of time, the double-slit experiment has been applied to demonstrate wave-particle duality for larger and larger compounds, and it is these paradoxical findings that have cemented the double-slit experiment in the foundation of quantum mechanics [3]. Thus, it was selected as a most excellent starting point for my endeavor.

1.3 The Copenhagen Interpretation

When performing computations with the Copenhagen interpretation, one is considering the classical world to be separate from the quantum world. The universe is divided into quantum mechanical phenomena and classical observers and apparatuses that interact with those phenomena. In this interpretation, the question of destroying interference is answered with the idea of measurement. Measurement and classical observers enter the Copenhagen interpretation with the projection postulate, which states that when an observable A is measured and found to take the value a, the system's state (initially $|\psi\rangle$) is projected (by the operator P_a^A) onto the states corresponding to the measured value and renormalized, becoming the new state $|\psi'\rangle$.

[4] Sorry, spoiler alert!

[5] Within limits, that is. The phenomenon of single-slit interference, often explained using the wavelets of Huygens' principle, arises when a diffracting wave exiting a single open slit interferes with itself to create a distinct fringe pattern [15]. Single-slit interference will come up again in Section 4.

This is known as state collapse, and is represented by the following formula [1]:

$$|\psi'\rangle = \frac{P_a^A |\psi\rangle}{\sqrt{\langle\psi|P_a^A|\psi\rangle}}. \tag{1.4}$$

In order to determine the probability of a particular measurement outcome, one applies the Born rule[6], which expresses the probability as the squared magnitude of the inner product of the state associated with the outcome (particularly $|a\rangle$) and the initial state [1]:

$$\mathscr{P}(a) = |\langle a|\psi\rangle|^2. \tag{1.5}$$

In the Copenhagen interpretation, it is the job of measurement to destroy interference and allow probabilities to be assigned. This is very limiting, however, since it requires us to have a classical domain in which the observer resides. Under this framework, we are unable to compute quantum mechanical probabilities without classical physics. We need to be able to assign probabilities to closed systems, and to demystify the ill-defined notion of measurement. But first, there is an intermediate step.

1.4 Extending Copenhagen

You can apply the Born rule and the collapse postulate together multiple times in succession to determine the probability of a sequence of events, but there is a slicker way. Consider a sequence of measurements on an arbitrary normalized state $|\psi\rangle$. First, the observable A is measured to have value a (one of its eigenvalues). According to the Born rule, the probability of this result is $\mathscr{P}(a) = |\langle a|\psi\rangle|^2$. Furthermore, following measurement, the initial state is projected into the eigenspace of a and renormalized. We have taken $|a\rangle$ to be the eigenstate associated with eigenvalue a, so it follows that the projector into the eigenspace is $P_a^A = |a\rangle\langle a|$, and the new state $|\psi'\rangle$ is obtained via the following computation:

$$|\psi'\rangle = \frac{P_a^A |\psi\rangle}{||P_a^A |\psi\rangle||}. \tag{1.6}$$

Here, I have shifted my notation away from my earlier expression of the projection postulate. The norm bars $||\cdot||$ indicate that we are taking a square root of a state's inner product with itself, i.e. the norm of $|\psi\rangle$ is $||\,|\psi\rangle\,|| = \sqrt{\langle\psi|\psi\rangle}$. In particular, $||P_a^A|\psi\rangle|| = \sqrt{\langle\psi|P_a^A P_a^A|\psi\rangle}$, which has an extra projection operator compared to Eqn. 1.4. This is resolved by the fact that the square of a projector is itself [17], so $(P_a^A)^2 = P_a^A$ and we arrive at exactly the form of Eqn. 1.4.

After measuring a, the observable B is found to have value b. The probability of this result given our earlier measurement of A turning out to be a is $\mathscr{P}(b|a) = |\langle b|\psi'\rangle|^2$. Note that $\mathscr{P}(b|a)$ is standard probability notation for the probability of event b given that a has occurred.

[6] First derived by Max Born in 1926 [16].

The probability of first a occurring, then b occurring (denoted $\mathscr{P}(b,a)$ to maintain the ordering seen in $\mathscr{P}(b|a)$), is the product of the probability of the first event and the probability of the second event given the first event happened:

$$\begin{aligned}\mathscr{P}(b,a) &= \mathscr{P}(b|a)\mathscr{P}(a) \\ &= |\langle b|\psi'\rangle|^2 |\langle a|\psi\rangle|^2 \\ &= \langle\psi'|b\rangle\langle b|\psi'\rangle\langle\psi|a\rangle\langle a|\psi\rangle .\end{aligned} \tag{1.7}$$

This expression can be manipulated, knowing that $\langle a|a\rangle = \langle b|b\rangle = 1$ and $||P|\psi\rangle|| = \sqrt{\langle\psi|PP|\psi\rangle}$.

$$\begin{aligned}\mathscr{P}(b,a) &= \langle\psi'|b\rangle\langle b|b\rangle\langle b|\psi'\rangle\langle\psi|a\rangle\langle a|a\rangle\langle a|\psi\rangle \\ &= \langle\psi'|P_b^B P_b^B|\psi'\rangle\langle\psi|P_a^A P_a^A|\psi\rangle \\ &= ||P_b^B|\psi'\rangle||^2 ||P_a^A|\psi\rangle||^2\end{aligned} \tag{1.8}$$

At this point, Eqn. 1.6 can be substituted in for $|\psi'\rangle$.

$$\begin{aligned}\mathscr{P}(b,a) &= \left|\left| P_b^B \frac{P_a^A|\psi\rangle}{||P_a^A|\psi\rangle||} \right|\right|^2 ||P_a^A|\psi\rangle||^2 \\ &= ||P_b^B P_a^A|\psi\rangle||^2 \\ &= \langle\psi|P_a^A P_b^B P_b^B P_a^A|\psi\rangle\end{aligned} \tag{1.9}$$

Unlike probabilities under the Born rule, this is not the squared magnitude of an inner product.[7] This formula—known as the *von Neumann-Lüders rule* and seen more generally in Ref. [18][8]—could be extended indefinitely, chaining projection operators together ad nauseam to represent a sequence of observation events and calculating the probability of experiencing the full sequence—one possible history of events, so to speak.

The tricky part is knowing when the probabilities you have calculated are applicable. In the case of the double slit experiment, let $\mathscr{P}(y,u)$ be the probability of the electron passing through the upper slit and then impacting a point y on the detector screen, and let $\mathscr{P}(y,l)$ be the probability of the electron passing through the lower slit and then impacting the same point on the detector screen. If we look at the total probability $\mathscr{P}(y)$ of the electron arriving at the point y, we find that $\mathscr{P}(y) \neq \mathscr{P}(y,u) + \mathscr{P}(y,l)$. In other words, we cannot construct the double-slit interference pattern by adding up the patterns produced by each slit individually. If a measurement of the electron's path is made, however, the total pattern will be the sum of two single-slit patterns, and therefore lacking the double-slit interference fringes. The consistent histories formalism includes the additional mathematics necessary to determine when a probability can be properly assigned to a sequence of events. In the Copenhagen interpretation, a measurement must be made to do so.

[7] However, if one were to consider a sequence with only one event in it, P_a^A, then it would reduce to the Born rule: $\mathscr{P}(a) = \langle\psi|P_a^A P_a^A|\psi\rangle = \langle\psi|a\rangle\langle a|a\rangle\langle a|\psi\rangle = \langle\psi|a\rangle\langle a|\psi\rangle = |\langle a|\psi\rangle|^2$.

[8] which is a translation of the original [19]

1.5 Quickly Formalizing the Formalism

A history h is a particular time-ordered set of projection events for a given system. A history can be *fine-grained*, which means that every instant is described in the history—nothing is left unaccounted for in the sequence of events the system experiences. This description is so exact, that fine-grained histories generally do not *decohere* (to be explained shortly). It is more practical to work with *coarse-grained* histories, which describe the important events for the system. In our above example, we used a coarse-grained history, namely:

$$h = \{P_a^A, P_b^B\}. \tag{1.10}$$

Note that the curly braces are set notation, meaning the two projectors are elements of h. For the purposes of our continuing discussion, let us add one more event, and specify the times at which these events occur:

$$h = \{P_a^A(t_1), P_b^B(t_2), P_c^C(t_3)\}. \tag{1.11}$$

This history describes observable A having value a at time t_1, observable B having value b at time t_2, and observable C having value c at time t_3. We consider this history to be coarse-grained because we do not specify the events between the indicated times. The nature of h as a branch on the metaphorical tree of possibility can be shown illustratively, as in Fig. 1.5.

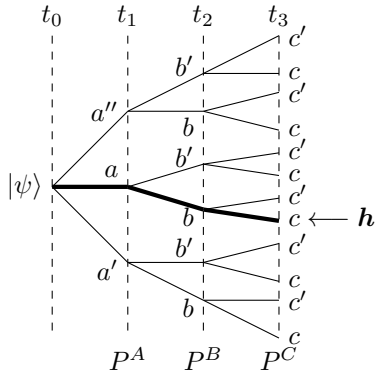

Figure 1.5: Branching Histories Here, we illustrate a set of histories in which an observable A (which can have the value a, a', or a'') is considered at time t_1, an observable B (which can have the value b or b') is considered at time t_2, and an observable C (which can have the value c or c') is considered at time t_3. Each path—or branch—represents a history in the set. The dark branch is the particular history h, wherein A takes value a at t_1, B takes value b at t_2, and C takes value c at t_3. Later, we will learn that being able to meaninfully assign probabilities to histories in a set such as this depends on whether or not the discrete branches evince quantum interference.

Later, when we want to perform calculations with our history, we will want it to be part of an exclusive, exhaustive set of histories. At each time in the system, we have an observable[9], and each observable has a

[9] Actually, we can have up to a complete set of commuting observables (CSCO) at each time, since we can know the outcomes of these observables simultaneously [1].

set of eigenvalues which are its allowed outcomes. For a set of histories to be exclusive and exhaustive, it must contain a history for each sequence of outcomes. For example, our family of histories from Fig. 1.5 has the following outcomes, grouped by time of applicability and represented by their associated projectors:

$$\left\{\{P_a^A(t_1), P_{a'}^A(t_1), P_{a''}^A(t_1)\}, \{P_b^B(t_2), P_{b'}^B(t_2)\}, \{P_c^C(t_3), P_{c'}^C(t_3)\}\right\}. \tag{1.12}$$

If we were to select one outcome for each time, say a' at t_1, b' at t_2 and c' at t_3, we would be able to represent it with a history from our family, particularly

$$\{P_{a'}^A(t_1), P_{b'}^B(t_2), P_{c'}^C(t_3)\}. \tag{1.13}$$

If there were not a history representing this path in the set, then the family from Fig. 1.5 would not be an exclusive and exhaustive set.

At each time, since all outcomes of the associated observable are accounted for in the exclusive, exhaustive family, we know that the sum of all available projection operators for that time is the identity. In our example,

$$\mathbb{I} = P_a^A + P_{a'}^A + P_{a''}^A, \tag{1.14a}$$

$$\mathbb{I} = P_b^B + P_{b'}^B, \tag{1.14b}$$

$$\mathbb{I} = P_c^C + P_{c'}^C. \tag{1.14c}$$

When we coarse-grain over a collection of outcomes to create a new family of histories, we are performing this addition of projectors. Regarding this, I have two examples. First, consider the family which selects from the following specifications:

$$\left\{\{P_a^A(t_1), P_{a'}^A(t_1) + P_{a''}^A(t_1)\}, \{P_b^B(t_2), P_{b'}^B(t_2)\}, \{P_c^C(t_3), P_{c'}^C(t_3)\}\right\}. \tag{1.15}$$

A history from this family can specify that A takes the value a, or it takes one of the two values a' or a''. No distinction is made between the latter two. More extremely, consider the family which selects from

$$\left\{\{\mathbb{I}(t_1)\}, \{P_b^B(t_2), P_{b'}^B(t_2)\}, \{P_c^C(t_3), P_{c'}^C(t_3)\}\right\}, \tag{1.16}$$

which does not allow its histories to specify a value for A at t_1 at all. For a history of this family, A is allowed to take any of its three possible values, but which one in particular occurs is not germane to the sequence of events. In our original family from Fig. 1.5, we have done this level of course-graining over all possibilities for times between those specified.

It is also important to point out that the consistent histories formalism operates in the Heisenberg picture, rather than the Schrödinger picture. This means that time-dependence is situated in the operators, rather than the wave function [17]. For some system with initial state $|\psi\rangle$ at time t_0, an operator O would be expressed

$$O(t) = U^\dagger(t, t_0) O U(t, t_0), \tag{1.17}$$

where O is the time-independent version of the operator and U is the propagator, a unitary linear operator (to be described more fully hereafter). The superscript dagger (†) indicates the Hermitian adjoint of an operator. In this picture, the projection operators in our current example would be

$$P_a^A(t_1) = U^\dagger(t_1, t_0) P_a^A U(t_1, t_0), \tag{1.18a}$$

$$P_b^B(t_2) = U^\dagger(t_2, t_0) P_b^B U(t_2, t_0), \tag{1.18b}$$

$$P_c^C(t_3) = U^\dagger(t_3, t_0) P_c^C U(t_3, t_0). \tag{1.18c}$$

A history can be expressed as a *class operator*, which is simply the time-ordered product of the projection operators of the associated history. In our earlier example, the class operator for the history h is

$$C_h = P_a^A(t_1) P_b^B(t_2) P_c^C(t_3). \tag{1.19}$$

The class operator can subsequently be applied to construct the *branch wave function*, which is the wave function of the system acted upon by all of the projectors. This is achieved by applying the Hermitian adjoint of the class operator.[10] The branch wave function of our example history h is

$$|\psi_h\rangle = C_h^\dagger |\psi\rangle = P_c^C(t_3) P_b^B(t_2) P_a^A(t_1) |\psi\rangle . \tag{1.20}$$

This is an excellent point to introduce some key properties of the propagator. First, as I already mentioned, the propagator is unitary, so its Hermitian adjoint is its inverse as well. Moreover, the inversion is achieved simply by reversing the time order:

$$U^\dagger(t_i, t_j) = U^{-1}(t_i, t_j) = U(t_j, t_i). \tag{1.21}$$

Second, if one takes the product of a propagator having time t_j listed second (namely $U(t_i, t_j)$) with another propagator having time t_j listed first (*viz.* $U(t_j, t_k)$), they merge to form the propagator $U(t_i, t_k)$. Since $U(t_j, t_k) = U^\dagger(t_k, t_j)$, the product of a propagator and an adjoint propagator both listing t_j second may also combine in this manner:

$$U(t_i, t_j) U(t_j, t_k) = U(t_i, t_k) = U(t_i, t_j) U^\dagger(t_k, t_j). \tag{1.22}$$

One can easily see how these properties work in a propagator for a time-independent Hamiltonian H, which can be expressed as

$$U(t_i, t_j) = e^{-iH(t_i - t_j)/\hbar}. \tag{1.23}$$

[10] This is but one convention. James Hartle defines the time-ordered class operator as $C_h^\dagger$ and the reverse-ordered operator for use on the wave function as C_h, exactly opposite the practice used here.[7]

This form is not generally true for a time-dependent Hamiltonian. The properties, however, are general, so we may use them to express the branch wave function as

$$\begin{aligned} |\psi_h\rangle &= U^\dagger(t_3,t_0)P_c^C U(t_3,t_0)U^\dagger(t_2,t_0)P_b^B U(t_2,t_0)U^\dagger(t_1,t_0)P_a^A U(t_1,t_0)\,|\psi\rangle \\ &= U(t_0,t_3)P_c^C U(t_3,t_2)P_b^B U(t_2,t_1)P_a^A U(t_1,t_0)\,|\psi\rangle\,. \end{aligned} \tag{1.24}$$

Here, one can see how the propagators (except for the strange backward one $U(t_0,t_3)$) move the state forward in time from one event to the next. Reading from right to left, we start in state $|\psi\rangle$ at t_0, then evolve to t_1, when P_a^A is applied. The system then evolves to t_2, when P_b^B is applied, and finally we move on to t_3, when P_c^C is applied. Note that, if we were to take the inner product $\langle\psi_h|\psi_h\rangle$ (perhaps we are applying the von Neumann-Lüders rule), the $U(t_0,t_3)$ in Eqn. 1.24 will cancel with its Hermitian adjoint. That particular propagator introduces an arbitrary global phase, and is really just an artifact of using the Heisenberg picture.

To analyze branch interference between different histories, one needs the *decoherence functional*. In its basic form, it can be expressed as simply the inner product of two branch wave functions:

$$d(h,h') = \langle\psi_{h'}|\psi_h\rangle = \langle\psi|C_{h'}C_h^\dagger|\psi\rangle\,. \tag{1.25}$$

This is valid for a pure initial state.[11] If we consider taking the decoherence functional of our history h from Eqn. 1.11 with itself, we find that

$$d(h,h) = \langle\psi_h|\psi_h\rangle = \langle\psi|C_hC_h^\dagger|\psi\rangle = \langle\psi|P_a^A(t_1)P_b^B(t_2)P_c^C(t_3)P_c^C(t_3)P_b^B(t_2)P_a^A(t_1)|\psi\rangle\,. \tag{1.26}$$

It is no coincidence that this results in the form of the von Neumann-Lüders rule, but don't get excited and call this a probability just yet.

If you have a set of histories $\{h\}$ which is exhaustive and exclusive, then the decoherence functional is normalized:

$$\sum_{h,h'} d(h,h') = 1. \tag{1.27}$$

If $d(h,h') \approx 0$ for all $h \neq h'$ (in other words, all branch wave functions representing distinct histories are orthogonal), then the set of histories is said to be *consistent*—in other words, the histories *decohere*. When a set of histories is consistent, the decoherence functional becomes diagonal, and each entry along its diagonal is the probability of a history of the set coming to pass:

$$d(h,h') = \delta_{h,h'}\mathscr{P}(h). \tag{1.28}$$

Notice the normalization of the decoherence functional is now the normalization of probabilities:

$$1 = \sum_{h,h'} d(h,h') = \sum_{h,h'} \delta_{h,h'}\mathscr{P}(h) = \sum_h \mathscr{P}(h). \tag{1.29}$$

[11] For a mixed state, the decoherence functional must be generalized in terms of a density matrix, ρ, and a trace: $d(h,h') = \mathrm{Tr}[C_h^\dagger \rho C_{h'}]$ [2, 7]. This form is not currently relevant.

It must be stressed that this is only valid for a consistent set. If $d(h, h') \neq 0$ for even one pair of histories, the decoherence functional remains normalized, but probabilities calculated by the von Neumann-Lüders rule do not add up correctly. It is no longer true that $\sum_h \mathscr{P}(h) = 1$, because some nonzero values are hiding in the off-diagonal elements of the decoherence functional.

In the Copenhagen interpretation, it is the role of measurement to validate probabilities. It is measurement which collapses states and removes interference between alternatives. In order to do quantum mechanics without relying on classical observers, the consistent histories formalism has generalized the idea of measurement. The decoherence functional is used to objectively measure quantum interference between alternatives, and as long as interference exists between histories in a set, we cannot assign meaningful probabilities.

The formalism is more carefully laid out in Refs. [2, 4], while one of the most in-depth treatments was given as lectures by James Hartle at Les Houches École d'eté in 1992 [7]. Now that we have the basic idea, we can use it as a lens to take a closer look at the double slit experiment.

Chapter 2

Emerging 2-Slit Interference

I shall be telling this with a sigh
Somewhere ages and ages hence:
Two slits diverged in a screen and I—
Can't tell which one I traveled by,
Because of branch interference.

—paraphrased from Robert Frost's *The Road Not Taken*

Now that we have all of the tools set out, we can ignite the forge and get to work on a specific case. First, we will hammer out the particulars of our double-slit system while it is still hot, defining its physical parameters and identifying the times, observables, and outcomes of all events. While that cools, we can cobble together the projectors we need for each outcome, then rivet them into the event chains we call branch wave functions. Operator by operator, the branch wave functions will be evaluated, pushing them toward forms which can be effectively examined using the decoherence functional. When all is said and done and the steam of the quenching has cleared, we will use what we have turned out to reproduce the interference pattern from Eqn. 1.3.

2.1 System Parameters

We begin with a system with time independent free-particle Hamiltonian H and with initial state $|\psi\rangle = |\vec{p}\rangle$, which is a momentum eigenstate. In the position basis, momentum eigenstates are plane waves:

$$\langle \vec{x}|\vec{p}\rangle = \frac{1}{\sqrt{2\pi\hbar}} e^{i\vec{p}\cdot\vec{x}/\hbar}. \tag{2.1}$$

Furthermore, since $\vec{p} = p_x\hat{x} + p_y\hat{y}$, the plane wave can be separated into an x-dependent part and a y-dependent part. Effectively, our initial state is a tensor product of momentum eigenstates:

$$|\psi\rangle = |p_x\rangle \otimes |p_y\rangle \doteq \frac{1}{2\pi\hbar} e^{ip_x x/\hbar} e^{ip_y y/\hbar}. \tag{2.2}$$

Note that the symbol $\doteq$ indicates that the mathematical object to the right is an expression of the object to the left in a particular basis [1]. Despite the symmetry of the symbol itself, $\doteq$ is not a symmetric relation; $\frac{1}{2\pi\hbar} e^{ip_x x/\hbar} e^{ip_y y/\hbar}$ represents $|p_x\rangle \otimes |p_y\rangle$ in the position basis, while $|p_x\rangle \otimes |p_y\rangle$ is a basis-independent object.

As depicted in Fig. 2.1, the first screen is encountered at time t_1. It has two slits in it, each Δy wide. The upper slit is centered at y_0, and the lower slit is centered at $-y_0$. The interval of the upper gap will be denoted by

$$\Delta u = \left[y_0 - \frac{\Delta y}{2}, y_0 + \frac{\Delta y}{2} \right] \tag{2.3}$$

while the interval of the lower gap will be denoted by

$$\Delta l = \left[-y_0 - \frac{\Delta y}{2}, -y_0 + \frac{\Delta y}{2} \right] \tag{2.4}$$

The detector screen is encountered at time t_2, and the particle collides with it at height y_f.

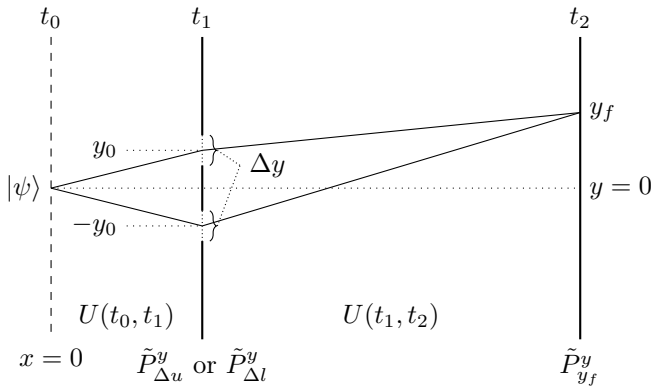

Figure 2.1: Double-Slit Apparatus In this figure, the x-axis is horizontal, and the y-axis is vertical. The incident wave function $|\psi\rangle$ passes through two slits at time t_1 and reaches height y_f on the detector screen at time t_2. The intervening moments during which the system undergoes unitary time evolution are marked by the associated propagators ($U(t_0, t_1)$ and $U(t_1, t_2)$). Both slits have width Δy, and their centers are separated by $2y_0$. The projectors associated with the slit interactions ($\tilde{P}^y_{\Delta u}$ and $\tilde{P}^y_{\Delta l}$) and the detector screen ($\tilde{P}^y_{y_f}$) are constructed in Section 2.2.

2.2 Constructing the Projectors

Each projector will have to be built up, first by constructing it in the state space it operates in (the y-direction), then by extending it into the full state space, and finally adding time dependence.

The projector for the detector screen is the simplest. Assuming infinite precision,[1] we can simply use the position eigenstate of the final position: $|y_f\rangle$. The base projector is

$$P^y_{y_f} = |y_f\rangle \langle y_f| . \tag{2.5}$$

This projector only operates in the state subspace associated with the y-direction, so its extension should have no effect on components of the system residing in the state subspace associated with the x-direction. This is accomplished through tensor product with the identity operator of the other subspace, making our extension

$$\tilde{P}^y_{y_f} = \mathbb{I}_x \otimes P^y_{y_f} = \int_{-\infty}^{\infty} dx\, |x\rangle \langle x| \otimes |y_f\rangle \langle y_f| . \tag{2.6}$$

As we can see here, the process of defining the identity here is analogous to defining the identity for a system with discrete eigenvalues. For a discrete spectrum, say spin-1/2, you add a complete set of projectors together as such:

$$\mathbb{I} = |+\rangle_z \, {}_z\langle +| + |-\rangle_z \, {}_z\langle -| \tag{2.7}$$

For a continuous spectrum like position, the addition is accomplished through integrating over the entire spectrum, as we did in Eqn. 2.6. Finally, the Heisenberg picture version (as we expressed in Equations 1.17 and 1.18) is

$$\tilde{P}^y_{y_f}(t_2) = U^\dagger(t_2, t_0) \tilde{P}^y_{y_f} U(t_2, t_0). \tag{2.8}$$

The first screen has two possible projection operators, one for each slit. Since each slit has finite (not infinitesimal) width, they can be classified as *insufficiently selective measurement devices* [17]. This means that all eigenvalues that are detected by the measurement device must be combined into a single projection operator that does not distinguish between them.[2] For our continuous position spectrum, this involves the integration we saw above. Thus, the projectors for the upper and lower slits are

$$P^y_{\Delta u} = \int_{\Delta u} dy\, |y\rangle \langle y| = \int_{y_0 - \frac{\Delta y}{2}}^{y_0 + \frac{\Delta y}{2}} dy\, |y\rangle \langle y| \text{ and } P^y_{\Delta l} = \int_{\Delta l} dy\, |y\rangle \langle y| = \int_{-y_0 - \frac{\Delta y}{2}}^{-y_0 + \frac{\Delta y}{2}} dy\, |y\rangle \langle y| . \tag{2.9}$$

It then follows that the extensions are

$$\tilde{P}^y_{\Delta u} = \mathbb{I}_x \otimes P^y_{\Delta u} = \int_{-\infty}^{\infty} dx\, |x\rangle \langle x| \otimes \int_{\Delta u} dy\, |y\rangle \langle y| \text{ and } \tilde{P}^y_{\Delta l} = \mathbb{I}_x \otimes P^y_{\Delta l} = \int_{-\infty}^{\infty} dx\, |x\rangle \langle x| \otimes \int_{\Delta l} dy\, |y\rangle \langle y| . \tag{2.10}$$

In the Heisenberg picture, these operators become

$$\tilde{P}^y_{\Delta u}(t_1) = U^\dagger(t_1, t_0) \tilde{P}^y_{\Delta u} U(t_1, t_0) \text{ and } \tilde{P}^y_{\Delta l}(t_1) = U^\dagger(t_1, t_0) \tilde{P}^y_{\Delta l} U(t_1, t_0). \tag{2.11}$$

[1] The mathematical limit of a point particle can only physically contact the screen at a single point. There is no reason to overcomplicate the detector screen with realistic notions of positional distinguishability. Besides, we will ultimately beget a probability density, which must be integrated over a non-infinitesimal region to get an actual probability.

[2] As such, insufficiently selective measurement devices are another form of coarse-graining.

2.3 Evaluating Branch Wave Functions

In terms of histories, h_u will denote the particle taking the path through the upper slit, and h_l will denote the particle taking the path through the lower slit:

$$h_u = \{\tilde{P}^y_{\Delta u}(t_1), \tilde{P}^y_{y_f}(t_2)\} \qquad h_l = \{\tilde{P}^y_{\Delta l}(t_1), \tilde{P}^y_{y_f}(t_2)\}. \tag{2.12}$$

The set $\{h_u, h_l\}$ describes the particle traversing a path to the detector screen through one of the two slits. It is my intention to evaluate the decoherence functional for this set in order to see if probabilities can be assigned to these paths.

These histories can be expressed as the class operators C_{h_u} and C_{h_l}:

$$C_{h_u} = \tilde{P}^y_{\Delta u}(t_1)\tilde{P}^y_{y_f}(t_2) = U^\dagger(t_1,t_0)\tilde{P}^y_{\Delta u}U(t_1,t_2)\tilde{P}^y_{y_f}U(t_2,t_0) \tag{2.13}$$

$$C_{h_l} = \tilde{P}^y_{\Delta l}(t_1)\tilde{P}^y_{y_f}(t_2) = U^\dagger(t_1,t_0)\tilde{P}^y_{\Delta l}U(t_1,t_2)\tilde{P}^y_{y_f}U(t_2,t_0). \tag{2.14}$$

It follows directly that the branch wave functions for the two paths, $|\psi_{h_u}\rangle$ and $|\psi_{h_l}\rangle$, are

$$|\psi_{h_u}\rangle = C^\dagger_{h_u}|\psi\rangle = U^\dagger(t_2,t_0)\tilde{P}^y_{y_f}U(t_2,t_1)\tilde{P}^y_{\Delta u}U(t_1,t_0)|\psi\rangle \tag{2.15}$$

and

$$|\psi_{h_l}\rangle = C^\dagger_{h_l}|\psi\rangle = U^\dagger(t_2,t_0)\tilde{P}^y_{y_f}U(t_2,t_1)\tilde{P}^y_{\Delta l}U(t_1,t_0)|\psi\rangle\,. \tag{2.16}$$

You may wonder why we do not consider two paths with differing endpoints, say y_f and y'_f. Notice that when one takes the decoherence functional of those two paths, the first product to evaluate—after $U(t_2,t_0)U^\dagger(t_2,t_0)$ cancels from the middle—is $\tilde{P}^y_{y'_f}\tilde{P}^y_{y_f}$. Once we take away the extension into the product space (which does nothing to the result here) and express the projectors in Dirac notation, we see that

$$P^y_{y'_f}P^y_{y_f} = |y'_f\rangle\langle y'_f|y_f\rangle\langle y_f|\,. \tag{2.17}$$

Since $\langle y'_f|y_f\rangle = 0$, the two histories decohere automatically. For our purposes, this is not the behavior we are interested in.

Let us first evaluate the effects of all operators in $|\psi_{h_u}\rangle$, one at a time. To begin, there is time evolution from the point of origin to the screen:

$$U(t_1,t_0)|\psi\rangle = e^{-iH(t_1-t_0)/\hbar}|p_x\rangle\otimes|p_y\rangle = e^{-i\frac{p_x^2+p_y^2}{2m}(t_1-t_0)/\hbar}|p_x\rangle\otimes|p_y\rangle\,. \tag{2.18}$$

As we can see, allowing the particle (in a momentum eigenstate) to evolve in free space only adds a global complex phase. Things start to get interesting at the first projector:

$$\tilde{P}^y_{\Delta u}U(t_1,t_0)|\psi\rangle = e^{-i\frac{p_x^2+p_y^2}{2m}(t_1-t_0)/\hbar}[\mathbb{I}_x\otimes P^y_{\Delta u}]|p_x\rangle\otimes|p_y\rangle = e^{-i\frac{p_x^2+p_y^2}{2m}(t_1-t_0)/\hbar}|p_x\rangle\otimes P^y_{\Delta u}|p_y\rangle\,. \tag{2.19}$$

Throughout, our coarse-graining of the x-component leaves $|p_x\rangle$ alone. The other half of the tensor product does not go undisturbed:

$$P^y_{\Delta u}|p_y\rangle = \int_{y_0-\frac{\Delta y}{2}}^{y_0+\frac{\Delta y}{2}} dy\,|y\rangle\,\langle y|p_y\rangle = \int_{y_0-\frac{\Delta y}{2}}^{y_0+\frac{\Delta y}{2}} dy\,|y\rangle\,\frac{1}{\sqrt{2\pi\hbar}}e^{ip_y y/\hbar}. \tag{2.20}$$

That last conversion is courtesy of the position space representation as presented in Eqn. 2.1. For now, we shall leave the integral unevaluated and move on to the second propagator:

$$U(t_2,t_1)\tilde{P}^y_{\Delta u}U(t_1,t_0)\,|\psi\rangle = e^{-i\frac{p_x^2+p_y^2}{2m}(t_1-t_0)/\hbar}e^{-iH(t_2-t_1)/\hbar}\,|p_x\rangle\otimes\int_{y_0-\frac{\Delta y}{2}}^{y_0+\frac{\Delta y}{2}} dy\,|y\rangle\,\frac{1}{\sqrt{2\pi\hbar}}e^{ip_y y/\hbar}. \tag{2.21}$$

From here, we must separate the Hamiltonian in terms of momentum operators:

$$H = \frac{\hat{p}_x^2}{2m}+\frac{\hat{p}_y^2}{2m}. \tag{2.22}$$

This allows us to split the propagator apart and more clearly apply it to the discrete parts of the tensor product state. The effect of $\hat{p}_y$ may require some thought, but the effect of $\hat{p}_x$ is quite easy to see:

$$\begin{aligned}U(t_2,t_1)\tilde{P}^y_{\Delta u}U(t_1,t_0)\,|\psi\rangle &= e^{-i\frac{p_x^2+p_y^2}{2m}(t_1-t_0)/\hbar}\exp\left[-i\frac{\hat{p}_x^2(t_2-t_1)}{2m\hbar}\right]|p_x\rangle\otimes e^{-i\frac{\hat{p}_y^2}{2m}(t_2-t_1)/\hbar}\int_{y_0-\frac{\Delta y}{2}}^{y_0+\frac{\Delta y}{2}} dy\,|y\rangle\,\frac{1}{\sqrt{2\pi\hbar}}e^{ip_y y/\hbar}\\ &= e^{-i\frac{p_x^2+p_y^2}{2m}(t_1-t_0)/\hbar}\exp\left[-i\frac{p_x^2(t_2-t_1)}{2m\hbar}\right]|p_x\rangle\otimes e^{-i\frac{\hat{p}_y^2}{2m}(t_2-t_1)/\hbar}\int_{y_0-\frac{\Delta y}{2}}^{y_0+\frac{\Delta y}{2}} dy\,|y\rangle\,\frac{1}{\sqrt{2\pi\hbar}}e^{ip_y y/\hbar}.\end{aligned} \tag{2.23}$$

The natural result is that the $\hat{p}_x$ operator in the exponential lost its hat, becoming the variable p_x. This gives us another global phase from the unaltered $|p_x\rangle$ part of the state. The $\hat{p}_y$ operator stayed the same, however, because its action on the integrated term is unclear. If we bring the evolution operator into the integral, we have the problem of how it affects a position eigenstate:

$$H|y\rangle = ?\implies e^{-i\frac{\hat{p}_y^2}{2m}(t_2-t_1)/\hbar}|y\rangle = ? \tag{2.24}$$

The solution lies in the vein of something done in Equations 2.6 and 2.7—that is to say, constructing an alternative statement of the identity:

$$\mathbb{I}_y = \int_{-\infty}^{\infty} dp'_y\,|p'_y\rangle\,\langle p'_y| \implies |y\rangle = \int_{-\infty}^{\infty} dp'_y\,|p'_y\rangle\,\langle p'_y|y\rangle\,. \tag{2.25}$$

With this, we can restate the position eigenstate in terms of momentum eigenstates, and the evolution operator will be applicable. Our result is

$$\begin{aligned}\int_{y_0-\frac{\Delta y}{2}}^{y_0+\frac{\Delta y}{2}} dy e^{-i\frac{\hat{p}_y^2}{2m}(t_2-t_1)/\hbar}\,|y\rangle\,\frac{1}{\sqrt{2\pi\hbar}}e^{ip_y y/\hbar} &= \int_{y_0-\frac{\Delta y}{2}}^{y_0+\frac{\Delta y}{2}} dy e^{-i\frac{\hat{p}_y^2}{2m}(t_2-t_1)/\hbar}\int_{-\infty}^{\infty} dp'_y\,|p'_y\rangle\,\langle p'_y|y\rangle\,\frac{1}{\sqrt{2\pi\hbar}}e^{ip_y y/\hbar}\\ &= \int_{y_0-\frac{\Delta y}{2}}^{y_0+\frac{\Delta y}{2}} dy\int_{-\infty}^{\infty} dp'_y e^{-i\frac{p'^2_y}{2m}(t_2-t_1)/\hbar}\,|p'_y\rangle\,\frac{1}{2\pi\hbar}e^{-ip'_y y/\hbar}e^{ip_y y/\hbar}.\end{aligned} \tag{2.26}$$

There is but one last operator we need to apply,[3] and that is $\tilde{P}^y_{y_f}$. Its effects are

$$\begin{aligned}
\tilde{P}^y_{y_f}U(t_2,t_1)\tilde{P}^y_{\Delta u}U(t_1,t_0)\left|\psi\right\rangle &= \left[\mathbb{I}_x\otimes\left|y_f\right\rangle\left\langle y_f\right|\right]e^{-i\frac{p_x^2+p_y^2}{2m}(t_1-t_0)/\hbar}e^{-i\frac{p_x^2}{2m}(t_2-t_1)/\hbar}\left|p_x\right\rangle \\
&\quad\otimes\int_{y_0-\frac{\Delta y}{2}}^{y_0+\frac{\Delta y}{2}}dy\int_{-\infty}^{\infty}dp'_y e^{-i\frac{p'^2_y}{2m}(t_2-t_1)/\hbar}\left|p'_y\right\rangle\frac{1}{2\pi\hbar}e^{-ip'_y y/\hbar}e^{ip_y y/\hbar} \\
&= \frac{1}{2\pi\hbar}e^{-i\frac{p_x^2+p_y^2}{2m}(t_1-t_0)/\hbar}e^{-i\frac{p_x^2}{2m}(t_2-t_1)/\hbar}\left|p_x\right\rangle \\
&\quad\otimes\int_{y_0-\frac{\Delta y}{2}}^{y_0+\frac{\Delta y}{2}}dy\int_{-\infty}^{\infty}dp'_y e^{-i\frac{p'^2_y}{2m}(t_2-t_1)/\hbar}\left|y_f\right\rangle\left\langle y_f|p'_y\right\rangle e^{-ip'_y y/\hbar}e^{ip_y y/\hbar} \\
&= \frac{1}{\sqrt{2\pi\hbar}^3}e^{-i\frac{p_x^2+p_y^2}{2m}(t_1-t_0)/\hbar}e^{-i\frac{p_x^2}{2m}(t_2-t_1)/\hbar}\left|p_x\right\rangle \\
&\quad\otimes\int_{y_0-\frac{\Delta y}{2}}^{y_0+\frac{\Delta y}{2}}dy\int_{-\infty}^{\infty}dp'_y e^{-i\frac{p'^2_y}{2m}(t_2-t_1)/\hbar}e^{ip'_y y_f/\hbar}e^{-ip'_y y/\hbar}e^{ip_y y/\hbar}\left|y_f\right\rangle .
\end{aligned} \tag{2.27}$$

After all of that,[4] we can now say

$$\left|\psi_{h_u}\right\rangle = U(t_0,t_2)\left[\frac{1}{\sqrt{2\pi\hbar}^3}e^{-i\frac{p_x^2}{2m}(t_2-t_0)/\hbar}e^{-i\frac{p_y^2}{2m}(t_1-t_0)/\hbar}\int_{y_0-\frac{\Delta y}{2}}^{y_0+\frac{\Delta y}{2}}dy\int_{-\infty}^{\infty}dp'_y e^{-i\frac{p'^2_y}{2m}(t_2-t_1)/\hbar}e^{ip'_y y_f/\hbar}e^{-ip'_y y/\hbar}e^{ip_y y/\hbar}\right]\left|p_x\right\rangle\otimes\left|y_f\right\rangle . \tag{2.28}$$

Our main objective now is to simplify the double integral

$$\int_{y_0-\frac{\Delta y}{2}}^{y_0+\frac{\Delta y}{2}}dy\int_{-\infty}^{\infty}dp'_y e^{-i\frac{p'^2_y}{2m}(t_2-t_1)/\hbar}e^{ip'_y y_f/\hbar}e^{-ip'_y y/\hbar}e^{ip_y y/\hbar}. \tag{2.29}$$

The order of taking the integrals is immaterial, but I found the present order to be least problematic. Let us move that complex exponential on the end out of the integrand and see what we are left with:

$$\begin{aligned}
\int_{-\infty}^{\infty}dp'_y e^{-i\frac{p'^2_y}{2m}(t_2-t_1)/\hbar}e^{ip'_y y_f/\hbar}e^{-ip'_y y/\hbar} &= \int_{-\infty}^{\infty}dp'_y\exp\left(-i\left[\frac{t_2-t_1}{2m\hbar}p'^2_y+\frac{y-y_f}{\hbar}p'_y\right]\right) \\
&= \int_{-\infty}^{\infty}dp'_y\exp\left(-i\left\{\left[\sqrt{\frac{t_2-t_1}{2m\hbar}}p'_y+\frac{y-y_f}{2\hbar}\sqrt{\frac{2m\hbar}{t_2-t_1}}\right]^2-\left(\frac{y-y_f}{2\hbar}\right)^2\frac{2m\hbar}{t_2-t_1}\right\}\right) \\
&= \exp\left(i\left(\frac{y-y_f}{2\hbar}\right)^2\frac{2m\hbar}{t_2-t_1}\right)\int_{-\infty}^{\infty}dp'_y\exp\left(-i\left[\sqrt{\frac{t_2-t_1}{2m\hbar}}p'_y+\frac{y-y_f}{2\hbar}\sqrt{\frac{2m\hbar}{t_2-t_1}}\right]^2\right).
\end{aligned} \tag{2.30}$$

It is my intention to get the integral into the form[5]

$$\int_{-\infty}^{\infty}e^{-ax^2}dx = \sqrt{\frac{\pi}{a}}. \tag{2.31}$$

In order to do this, we will make the substitution

$$p''_y = \sqrt{\frac{t_2-t_1}{2m\hbar}}p'_y+\frac{y-y_f}{2\hbar}\sqrt{\frac{2m\hbar}{t_2-t_1}} \implies dp''_y = \sqrt{\frac{t_2-t_1}{2m\hbar}}dp'_y. \tag{2.32}$$

[3] As I have mentioned before, the last propagator will cancel when inner products are taken, so there is little reason to bother applying effort on the matter.

[4] and after redistributing the global phase to combine instances of p_x,

[5] This form is adapted from Eqn. F.22 on page 550 of McIntyre's textbook [1].

With this, we end up with the simple evaluation

$$\exp\left(i\left(\frac{y-y_f}{2\hbar}\right)^2\frac{2m\hbar}{t_2-t_1}\right)\sqrt{\frac{2m\hbar}{t_2-t_1}}\int_{-\infty}^{\infty}dp_y''e^{-ip_y''^2}=\exp\left(i\left(\frac{y-y_f}{2\hbar}\right)^2\frac{2m\hbar}{t_2-t_1}\right)\sqrt{\frac{2m\hbar}{t_2-t_1}}\sqrt{\frac{\pi}{i}}. \quad (2.33)$$

The outer integral remains to be done. Substituting Eqn. 2.33 into Eqn. 2.29 begets

$$\sqrt{\frac{2m\hbar}{t_2-t_1}}\sqrt{\frac{\pi}{i}}\int_{y_0-\frac{\Delta y}{2}}^{y_0+\frac{\Delta y}{2}}dy\exp\left(i\left[\left(\frac{y-y_f}{2\hbar}\right)^2\frac{2m\hbar}{t_2-t_1}+\frac{p_y y}{\hbar}\right]\right). \quad (2.34)$$

Since the bounds of integration do not cover all of space, this cannot be solved in the manner of the inner integral. However, it will still behoove us to make rearrangements as though we intended to solve it in that way. To begin, we must rearrange the argument of our remaining complex exponential:

$$\begin{aligned}\left(\frac{y-y_f}{2\hbar}\right)^2\frac{2m\hbar}{t_2-t_1}+\frac{p_y y}{\hbar}&=\frac{m}{2\hbar(t_2-t_1)}y^2+\left(\frac{p_y}{\hbar}-\frac{my_f}{\hbar(t_2-t_1)}\right)y+\frac{my_f^2}{2\hbar(t_2-t_1)}\\&=\left[\sqrt{\frac{m}{2\hbar(t_2-t_1)}}y+\frac{1}{2}\sqrt{\frac{2\hbar(t_2-t_1)}{m}}\left(\frac{p_y}{\hbar}-\frac{my_f}{\hbar(t_2-t_1)}\right)\right]^2\\&\quad+\frac{my_f^2}{2\hbar(t_2-t_1)}-\frac{\hbar(t_2-t_1)}{2m}\left(\frac{p_y}{\hbar}-\frac{my_f}{\hbar(t_2-t_1)}\right)^2.\end{aligned} \quad (2.35)$$

Let us expand and simplify the material outside of the square brackets:

$$\begin{aligned}\frac{my_f^2}{2\hbar(t_2-t_1)}-\frac{\hbar(t_2-t_1)}{2m}\left(\frac{p_y}{\hbar}-\frac{my_f}{\hbar(t_2-t_1)}\right)^2&=\frac{my_f^2}{2\hbar(t_2-t_1)}-\frac{\hbar(t_2-t_1)}{2m}\left(\frac{p_y^2}{\hbar^2}-\frac{2p_y my_f}{\hbar^2(t_2-t_1)}+\frac{m^2y_f^2}{\hbar^2(t_2-t_1)^2}\right)\\&=\frac{p_y y_f}{\hbar}-\frac{p_y^2}{2m\hbar}(t_2-t_1).\end{aligned} \quad (2.36)$$

Thus, the outer exponential becomes the product of a plane wave and a piece of evolution-like phase. Our integral becomes

$$\sqrt{\frac{2m\hbar}{t_2-t_1}}\sqrt{\frac{\pi}{i}}e^{-i\frac{p_y^2}{2m}(t_2-t_1)/\hbar}e^{ip_y y_f/\hbar}\int_{y_0-\frac{\Delta y}{2}}^{y_0+\frac{\Delta y}{2}}dy\exp\left(i\left[\sqrt{\frac{m}{2\hbar(t_2-t_1)}}y+\frac{1}{2}\sqrt{\frac{2\hbar(t_2-t_1)}{m}}\left(\frac{p_y}{\hbar}-\frac{my_f}{\hbar(t_2-t_1)}\right)\right]^2\right). \quad (2.37)$$

If we then apply the substitution

$$y'=\sqrt{\frac{m}{2\hbar(t_2-t_1)}}y+\frac{1}{2}\sqrt{\frac{2\hbar(t_2-t_1)}{m}}\left(\frac{p_y}{\hbar}-\frac{my_f}{\hbar(t_2-t_1)}\right)\implies dy'=\sqrt{\frac{m}{2\hbar(t_2-t_1)}}dy, \quad (2.38)$$

our integral simplifies to

$$2\hbar\sqrt{\frac{\pi}{i}}e^{-i\frac{p_y^2}{2m}(t_2-t_1)/\hbar}e^{ip_y y_f/\hbar}\int_{\Delta u'}dy'\exp\left(iy'^2\right), \quad (2.39)$$

where $\Delta u'$ is the altered region of integration. Here, we can quickly check our work by assuming $\Delta y=\infty$. The new bounds are from $-\infty$ to ∞, so the value of the integral becomes $\sqrt{\frac{\pi}{-i}}$ as per Eqn. 2.31. Thus, the former double integral simplifies to

$$2\pi\hbar e^{-i\frac{p_y^2}{2m}(t_2-t_1)/\hbar}e^{ip_y y_f/\hbar}. \quad (2.40)$$

Substituting this into Eqn. 2.28, we get

$$|\psi_{h_u}\rangle = U(t_0,t_2)\left[\frac{1}{\sqrt{2\pi\hbar}}e^{ip_y y_f/\hbar}e^{-i\frac{p_x^2+p_y^2}{2m}(t_2-t_0)/\hbar}\right]|p_x\rangle\otimes|y_f\rangle\,, \tag{2.41}$$

which is equivalent to the history we would construct by removing the screen with slits entirely:

$$U(t_0-t_2)\tilde{P}^y_{y_f}U(t_2-t_0)\,|p_x\rangle\otimes|p_y\rangle\,. \tag{2.42}$$

In order to solve our integral without removing the slits, let us return to Eqn. 2.37. If we assume that $\lambda \gg \Delta y$, then the slits are practically point sources on the scale of the wavelength. As such, the integrand of Eqn. 2.37 will not vary particularly much over the interval Δu, and we can make the estimation

$$\int_{y_0-\frac{\Delta y}{2}}^{y_0+\frac{\Delta y}{2}} dy f(y) = \Delta y f(y_0). \tag{2.43}$$

Using the deBroglie wavelength relation ($\lambda_{dB} = \frac{h}{p}$), we can more explicitly state that the condition for this estimate is

$$\Delta y \ll \frac{2\pi\hbar}{\sqrt{p_x^2+p_y^2}}. \tag{2.44}$$

If we take this to be true, then Eqn. 2.37 becomes

$$\sqrt{\frac{2m\hbar}{t_2-t_1}}\sqrt{\frac{\pi}{i}}e^{-i\frac{p_y^2}{2m}(t_2-t_1)/\hbar}e^{ip_y y_f/\hbar}\Delta y\exp\left(i\left[\sqrt{\frac{m}{2\hbar(t_2-t_1)}}y_0+\frac{1}{2}\sqrt{\frac{2\hbar(t_2-t_1)}{m}}\left(\frac{p_y}{\hbar}-\frac{my_f}{\hbar(t_2-t_1)}\right)\right]^2\right). \tag{2.45}$$

Inserting this into Eqn. 2.28 and simplifying the coefficients, we can express the branch history passing through the upper slit as

$$|\psi_{h_u}\rangle = U(t_0,t_2)\left[\frac{\Delta y\sqrt{m}}{2\pi\hbar\sqrt{i(t_2-t_1)}}e^{-i\frac{p_x^2+p_y^2}{2m}(t_2-t_0)/\hbar}e^{ip_y y_f/\hbar}e^{i\left[\sqrt{\frac{m}{2\hbar(t_2-t_1)}}y_0+\frac{1}{2}\sqrt{\frac{2\hbar(t_2-t_1)}{m}}\left(\frac{p_y}{\hbar}-\frac{my_f}{\hbar(t_2-t_1)}\right)\right]^2}\right]|p_x\rangle\otimes|y_f\rangle\,. \tag{2.46}$$

The branch history passing through the lower slit only differs by bounds of integration, so it can be expressed as

$$|\psi_{h_l}\rangle = U(t_0,t_2)\left[\frac{\Delta y\sqrt{m}}{2\pi\hbar\sqrt{i(t_2-t_1)}}e^{-i\frac{p_x^2+p_y^2}{2m}(t_2-t_0)/\hbar}e^{ip_y y_f/\hbar}e^{i\left[\sqrt{\frac{m}{2\hbar(t_2-t_1)}}(-y_0)+\frac{1}{2}\sqrt{\frac{2\hbar(t_2-t_1)}{m}}\left(\frac{p_y}{\hbar}-\frac{my_f}{\hbar(t_2-t_1)}\right)\right]^2}\right]|p_x\rangle\otimes|y_f\rangle\,. \tag{2.47}$$

Now that we have our evaluated branch wave functions, we will need to know their inner products, both with themselves and with each other. In either case, the remaining evolution operator, as well as the phases $e^{-i\frac{p_x^2+p_y^2}{2m}(t_2-t_0)/\hbar}$ and $e^{ip_y y_f/\hbar}$, will be canceled out by their own conjugates. In the more specific cases of the decoherence functional, $d(h_u,h_u)$ and $d(h_l,h_l)$, the remaining complex exponential may also cancel with its own conjugate, leaving the result

$$d(h_u,h_u) = \langle\psi_{h_u}|\psi_{h_u}\rangle = \frac{\Delta y\sqrt{m}}{2\pi\hbar\sqrt{-i(t_2-t_1)}}\frac{\Delta y\sqrt{m}}{2\pi\hbar\sqrt{i(t_2-t_1)}}\langle p_x|p_x\rangle\langle y_f|y_f\rangle = \frac{m\Delta y^2}{4\pi^2\hbar^2(t_2-t_1)} \tag{2.48}$$

for the upper slit branch, and the identical result

$$d(h_l, h_l) = \langle \psi_{h_l} | \psi_{h_l} \rangle = \frac{m\Delta y^2}{4\pi^2 \hbar^2 (t_2 - t_1)} \tag{2.49}$$

for the lower slit branch. This same value appears as a coefficient when we take $d(h_u, h_l)$, but the slightly differing complex exponentials interact differently:

$$\begin{aligned} & e^{-i\left[\sqrt{\frac{m}{2\hbar(t_2-t_1)}}(-y_0)+\frac{1}{2}\sqrt{\frac{2\hbar(t_2-t_1)}{m}}\left(\frac{p_y}{\hbar}-\frac{my_f}{\hbar(t_2-t_1)}\right)\right]^2} e^{i\left[\sqrt{\frac{m}{2\hbar(t_2-t_1)}}y_0+\frac{1}{2}\sqrt{\frac{2\hbar(t_2-t_1)}{m}}\left(\frac{p_y}{\hbar}-\frac{my_f}{\hbar(t_2-t_1)}\right)\right]^2} \\ &= e^{-i\left[\frac{m}{2\hbar(t_2-t_1)}y_0^2-\left(\frac{p_y}{\hbar}-\frac{my_f}{\hbar(t_2-t_1)}\right)y_0+\frac{1}{2}\frac{\hbar(t_2-t_1)}{m}\left(\frac{p_y}{\hbar}-\frac{my_f}{\hbar(t_2-t_1)}\right)^2\right]} e^{i\left[\frac{m}{2\hbar(t_2-t_1)}y_0^2+\left(\frac{p_y}{\hbar}-\frac{my_f}{\hbar(t_2-t_1)}\right)y_0+\frac{1}{2}\frac{\hbar(t_2-t_1)}{m}\left(\frac{p_y}{\hbar}-\frac{my_f}{\hbar(t_2-t_1)}\right)^2\right]} \\ &= e^{i\left(\frac{p_y}{\hbar}-\frac{my_f}{\hbar(t_2-t_1)}\right)2y_0}. \end{aligned} \tag{2.50}$$

As such, the remaining, off-diagonal element of the decoherence functional becomes

$$d(h_u, h_l) = \langle \psi_{h_l} | \psi_{h_u} \rangle = \frac{m\Delta y^2}{4\pi^2 \hbar^2 (t_2 - t_1)} e^{i\left(\frac{p_y}{\hbar}-\frac{my_f}{\hbar(t_2-t_1)}\right)2y_0}. \tag{2.51}$$

Note that this is nonzero, which means that the histories h_u and h_l do not decohere, so Eqn. 2.48 and Eqn. 2.49 do not represent probabilities. We cannot assign probabilities to sets of histories that are not consistent.

If we instead consider a branch wave function in which we do not specify which slit the particle passes through (in other words, we coarse-grain out this information), we can construct a consistent set. The class operator for this history, h_{ul}, is

$$C_{h_{ul}} = U(t_0, t_1)\left[\tilde{P}^y_{\Delta u} + \tilde{P}^y_{\Delta l}\right] U(t_1, t_2) \tilde{P}^y_{y_f} U(t_2, t_0). \tag{2.52}$$

You may notice that this is equivalent to the sum of our two previous class operators: $C_{h_{ul}} = C_{h_u} + C_{h_l}$ (see Eqns. 2.13 and 2.14). The branch wave function $|\psi_{h_{ul}}\rangle = C^\dagger_{h_{ul}} |\psi\rangle$ is part of a consistent set; the only alternative paths differ by endpoint y_f, and we already know that these decohere (see Eqn. 2.17). When we evaluate the decoherence functional $d(h_{ul}, h_{ul})$, we obtain an actual probability associated with taking the expressed path. Since the path is specified by its endpoint, it is better for us to denote this probability as $\mathscr{P}(y_f)$, rather than $\mathscr{P}(h_{ul})$:

$$\begin{aligned} \mathscr{P}(y_f) = d(h_{ul}, h_{ul}) &= \langle \psi_{h_{ul}} | \psi_{h_{ul}} \rangle = \langle \psi | C_{h_{ul}} C^\dagger_{h_{ul}} | \psi \rangle \\ &= \langle \psi | \left[C_{h_u} + C_{h_l}\right] \left[C^\dagger_{h_u} + C^\dagger_{h_l}\right] | \psi \rangle \\ &= \langle \psi | C_{h_u} C^\dagger_{h_u} | \psi \rangle + \langle \psi | C_{h_u} C^\dagger_{h_l} | \psi \rangle + \langle \psi | C_{h_l} C^\dagger_{h_u} | \psi \rangle + \langle \psi | C_{h_l} C^\dagger_{h_l} | \psi \rangle \\ &= \langle \psi_{h_u} | \psi_{h_u} \rangle + \langle \psi_{h_u} | \psi_{h_l} \rangle + \langle \psi_{h_l} | \psi_{h_u} \rangle + \langle \psi_{h_l} | \psi_{h_l} \rangle . \end{aligned} \tag{2.53}$$

We already know all of these values! They are $d(h_u, h_u)$, $d(h_u, h_l)$ (regular and conjugated), and $d(h_l, h_l)$.

With some liberal factoring, we can see that

$$\begin{aligned}\mathscr{P}(y_f) &= \frac{m\Delta y^2}{4\pi^2\hbar^2(t_2-t_1)} + \frac{m\Delta y^2}{4\pi^2\hbar^2(t_2-t_1)}e^{-i\left(\frac{p_y}{\hbar}-\frac{my_f}{\hbar(t_2-t_1)}\right)2y_0} + \frac{m\Delta y^2}{4\pi^2\hbar^2(t_2-t_1)}e^{i\left(\frac{p_y}{\hbar}-\frac{my_f}{\hbar(t_2-t_1)}\right)2y_0} + \frac{m\Delta y^2}{4\pi^2\hbar^2(t_2-t_1)} \\ &= \frac{m\Delta y^2}{2\pi^2\hbar^2(t_2-t_1)}\left[1+\cos\left(\left(\frac{p_y}{\hbar}-\frac{my_f}{\hbar(t_2-t_1)}\right)2y_0\right)\right].\end{aligned} \tag{2.54}$$

Already, there is a resemblance to Eqn. 1.3. To make this similarity more complete, we will need some assumptions, as well as careful geometric reasoning. When the distance to the screen Δx is much larger

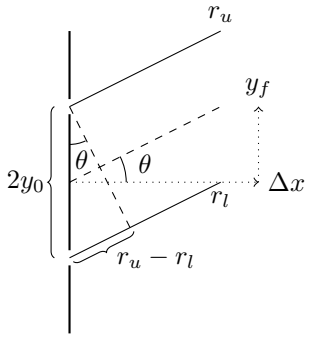

Figure 2.2: Geometry of Double-Slit Interference The paths r_u and r_l are nearly parallel when Δx (the distance to the detector screen) greatly exceeds $2y_0$. In this situation, the path length difference $r_u - r_l$ is about equal to $2y_0 \sin\theta$.

than the slit spacing $2y_0$, then the paths r_u and r_l are approximately parallel. These paths (as well as the dashed line from $y = 0$ on the first screen to $y = y_f$ on the detector screen on Fig. 2.2) make an angle θ with the horizontal. We can see from the figure that $\tan\theta = \frac{y_f}{\Delta x}$ and $\sin\theta = \frac{r_u - r_l}{2y_0}$. Within the bounds of the small-angle approximation, it can be said that $\theta \approx \sin\theta \approx \tan\theta$, so we can make the equivalence

$$\frac{r_u - r_l}{2y_0} \approx \frac{y_f}{\Delta x}. \tag{2.55}$$

Going back to Eqn. 2.54, we can use the above relation to replace $2y_f y_0$ and restate the cosine's argument:

$$\cos\left(\left(\frac{p_y}{\hbar}-\frac{my_f}{\hbar(t_2-t_1)}\right)2y_0\right) \approx \cos\left(\frac{p_y}{\hbar}2y_0 - \frac{m\Delta x(r_u-r_l)}{\hbar(t_2-t_1)}\right). \tag{2.56}$$

Now, dividing the distance Δx between the two screens by the travel time $t_2 - t_1$ gives the average velocity along the x-direction, and multiplying by the mass of the particle turns this into the average momentum along the x-direction. Throughout, the momentum eigenstate $|p_x\rangle$ has remained unchanged, and since a constant momentum is its own average, I propose we make the approximation

$$p_x \approx \frac{m\Delta x}{t_2 - t_1}, \tag{2.57}$$

which further alters the cosine to be

$$\cos\left(\frac{p_y}{\hbar}2y_0 - \frac{m\Delta x(r_u-r_l)}{\hbar(t_2-t_1)}\right) \approx \cos\left(\frac{p_y}{\hbar}2y_0 - \frac{p_x}{\hbar}(r_u-r_l)\right) = \cos\left(\frac{p_y}{\hbar}2y_0 - 2\pi\frac{p_x}{h}(r_u-r_l)\right). \tag{2.58}$$

Notice that a nonzero p_y means that the particle has some velocity parallel to the screen. Generally, one performs this experiment by aiming the light directly at the screen, so let us assume that $p_y = 0$, which further implies that p_x is the total velocity of the particle. This is why I made the substitution $\hbar = \frac{h}{2\pi}$ in Eqn. 2.58. That way, we can make the replacement $\lambda_{dB} = \frac{h}{p_x}$, turning the cosine into

$$\cos\left(\frac{p_y}{\hbar}2y_0 - 2\pi\frac{p_x}{h}(r_u - r_l)\right) \approx \cos\left(-2\pi\frac{r_u - r_l}{\lambda_{dB}}\right). \tag{2.59}$$

We can remove the negative sign inside, since cosine is an even function. Thus, the decoherence functional from Eqn. 2.54 takes its final form:

$$d(h_{ul}, h_{ul}) \approx \frac{m\Delta y^2}{2\pi^2\hbar^2(t_2 - t_1)}\left[1 + \cos\left(2\pi\frac{r_u - r_l}{\lambda_{dB}}\right)\right] = \mathscr{P}(y_f). \tag{2.60}$$

Now we have an exact match for Eqn. 1.3.

Upon initial inspection, there is reason to be concerned that Eqn. 2.60 has dimensions of inverse angular momentum. Since the histories decohere, the decoherence functional should be giving us a probability, right? Aren't probabilities dimensionless? First, our selection of possible outcomes is actually a continuous spectrum, so one necessarily must obtain a probability *density*. I apologize if I have been careless about interchanging the two terms, as it is an important distinction. Probability densities have dimensions inverse to the dimensions of the outcome spectrum, that way one must integrate over a selection of outcomes with nonzero width to get a probability of the outcome falling within a region.

Since $\mathscr{P}(y_f)$ has positions as outcomes, it ought to have dimensions of inverse length. The projector $P^y_{y_f} = |y_f\rangle\langle y_f|$ bears dimensions of inverse length, and it must be integrated over a range of positions to remove said dimensions (whereas $P^y_{\Delta u}$ and $P^y_{\Delta l}$ are already integrals of position eigenstates). However, that does not explain the dimensions of inverse angular momentum. For that, we go back to Eqn. 2.1. Our initial state is a momentum eigenstate, part of a continuous spectrum, which means it is a dimensionful quantity just like the position eigenstates. As such, we would have to introduce a normalization factor (with dimensions of momentum) to make up for this fine-grained specification.

There is one issue with attempting to normalize our probability density. Note that neither Eqn. 2.60 nor Eqn. 1.3 decays with distance from the slits. Both depend solely on path length difference, which approaches the limit of the slit spacing $2y_0$ as y_f approaches $\pm\infty$. If the slit spacing is not a half-integer multiple of the deBroglie wavelength, then the probability density will approach a finite number as the field point gets farther from the slits. This would lead to an infinite area beneath the curve, which cannot possibly be normalized. Since decay is absent from both the wave optics result and the quantum mechanical result, we cannot normalize either at this juncture.

Chapter 3

Don't Blink—Path Detection

An important facet of the double-slit experiment is its demonstration of the principle of complementarity. We see an interference pattern when both slits are open—as long as we do not attempt to divine which slit the particle goes through. On the other hand, if we include a path detector, we ought to lose the interference pattern [3].

We begin this chapter by considering the principles of detector models and presenting the intended outcome. Afterward, we move from the abstract to the concrete, applying a specific detector model to our system and making our original histories h_u and h_l into a consistent set. Finally, we spend a short time playing with the detector model, making it record incomplete information and examining the impact on the interference pattern as we transition from no which-way knowledge to a perfect record.

3.1 On the Nature of Detectors

If we want to add a detector, we must expand the original state space of our system, $\mathscr{H}_S$, to include the state space of the detector, $\mathscr{H}_D$. Together, they make the product space $\mathscr{H}_S \otimes \mathscr{H}_D$. Initially, we start with our system's initial state $|\psi\rangle$ uncorrelated with the detector's initial state $|D\rangle$:

$$|\Psi\rangle = |\psi\rangle \otimes |D\rangle = |p_x\rangle \otimes |p_y\rangle \otimes |D\rangle \,. \tag{3.1}$$

When the detector is in play, its states become correlated with the states of the system [20]. As such, our Hamiltonian for the product system must perform this operation as part of the time evolution of the system. When the particle passes through the slits at t_1, the history with the particle passing through the upper slit will be correlated with the upper slit detector state $|D_u\rangle$, while the history with the particle passing through the lower slit will be correlated with the lower slit detector state $|D_l\rangle$:

$$\tilde{P}^y_{\Delta u}(t_1)\,|\Psi\rangle = U^\dagger(t_1,t_0)\tilde{P}^y_{\Delta u}U(t_1,t_0)\,[|\psi\rangle \otimes |D\rangle] = U^\dagger(t_1,t_0)e^{-i\frac{p_x^2+p_y^2}{2m}(t_1-t_0)/\hbar}\left[\tilde{P}^y_{\Delta u}\,|\psi\rangle \otimes |D_u\rangle\right], \tag{3.2}$$

$$\tilde{P}^y_{\Delta l}(t_1)\,|\Psi\rangle = U^\dagger(t_1,t_0)e^{-i\frac{p_x^2+p_y^2}{2m}(t_1-t_0)/\hbar}\left[\tilde{P}^y_{\Delta l}\,|\psi\rangle\otimes|D_l\rangle\right]. \tag{3.3}$$

Note, I am being a tiny bit sloppy with the notation. Since the product space has expanded to include the detector, the product space extensions of the projectors must include an extra identity operator: $\mathbb{I}_x\otimes P^y_{\Delta u}\otimes\mathbb{I}_D$. However, after the last equality signs in Eqns. 3.2 and 3.3, the projector's extension takes its original meaning: $\mathbb{I}_x\otimes P^y_{\Delta u}$.

Ultimately, we are seeing the following transformation under the new Hamiltonian:

$$|\Psi\rangle = |\psi\rangle\otimes|D\rangle \longrightarrow \begin{cases} C^\dagger_{h_u}\,|\psi\rangle\otimes|D_u\rangle = |\psi_{h_u}\rangle\otimes|D_u\rangle \\ C^\dagger_{h_l}\,|\psi\rangle\otimes|D_l\rangle = |\psi_{h_l}\rangle\otimes|D_l\rangle\,. \end{cases} \tag{3.4}$$

As a physical analogy, consider a device with a dial on it, like an analog pressure gauge. When the particle goes through the slits, the dial arm either clicks to the right to point at a big capital U, or to the left to point at a big capital L. Which one it points at depends on which slit the particle transited. When it points to U, this is the detector state $|D_u\rangle$, indicating that the particle has passed through the upper slit. When it points to L, this is the detector state $|D_l\rangle$, indicating that the particle has passed through the lower slit.

If the detector states are orthogonal (that is to say, $\langle D_l|D_u\rangle = 0$), as is generally the case, we end up with a consistent set of histories:

$$d(h_u,h_l) = \langle\psi_{h_l}|\psi_{h_u}\rangle\,\langle D_l|D_u\rangle = 0. \tag{3.5}$$

This means that we can distinguish between the two histories unambiguously, and each has a probability associated with it, as given earlier in Eqns. 2.48 and 2.49:

$$\mathscr{P}(h_u) = d(h_u,h_u) = \frac{m\Delta y^2}{4\pi^2\hbar^2(t_2-t_1)}, \tag{3.6}$$

$$\mathscr{P}(h_l) = d(h_l,h_l) = \frac{m\Delta y^2}{4\pi^2\hbar^2(t_2-t_1)}. \tag{3.7}$$

3.2 An Explicit Model

We have demonstrated what we ought to see from a logical standpoint, but is it possible to construct an explicit Hamiltonian which produces this same effect? Indeed, this was done by Jonathan Halliwell as he explored the relationship between decoherence and stored information [21]. In short, one can refine the oft-repeated notion that *observation changes the observed*, as it is the existence of a persistent record which causes—so to speak—a system's histories to decohere. If the sequence of events within the system can be reconstructed from information in the environment, then the interference pattern will vanish.

To that end, we borrow Halliwell's example of a two-state environment, $\{|0\rangle\,,|1\rangle\}$, expanding our initial state into

$$|\Psi\rangle = |\psi\rangle\otimes|0\rangle = |p_x\rangle\otimes|p_y\rangle\otimes|0\rangle\,, \tag{3.8}$$

where $|0\rangle$ is the initial detector state, orthogonal to the other detector state $|1\rangle$. In addition, we define the action of the raising and lowering operators:

$$a\,|0\rangle = 0, \qquad a\,|1\rangle = |0\rangle\,, \qquad a^\dagger\,|0\rangle = |1\rangle\,, \qquad a^\dagger\,|1\rangle = 0. \tag{3.9}$$

We also define a window function:

$$\Upsilon(y) = \begin{cases} 1 & y \in \Delta u \\ 0 & y \notin \Delta u \end{cases}. \tag{3.10}$$

With these, we can define a new Hamiltonian, which is an augmentation of the free particle Hamiltonian H, now including an interaction with the detector:

$$\tilde{H}(t) = H + \lambda\delta(t - t_1)(a + a^\dagger)\Upsilon(y). \tag{3.11}$$

The coefficient λ is related to the coupling of the detector to the system, and we shall see later that it ought to equal $\frac{\pi\hbar}{2}$ for a perfectly correlated detector. The Dirac δ-function included in the Hamiltonian causes the raising and lowering operators to act only at time t_1, and thanks to the window function, only in a history where the particle is in Δu (that is to say, passes through the upper slit). The operator $a + a^\dagger$ flips the detector state completely (particularly, $(a+a^\dagger)\,|0\rangle = |1\rangle$, and vice versa), so if the particle transits the upper slit at t_1, it will interact with the detector and change the detector state.

To properly evaluate the action of this Hamiltonian on the detector, we would do well to know what the eigenstates of $a + a^\dagger$ are. The first, with an eigenvalue of $+1$, is

$$|{+1}\rangle = \frac{1}{\sqrt{2}}\left(|0\rangle + |1\rangle\right), \tag{3.12}$$

and the second, with an eigenvalue of -1, is

$$|{-1}\rangle = \frac{1}{\sqrt{2}}\left(|0\rangle - |1\rangle\right). \tag{3.13}$$

As such, we may express the detector states as a linear combination of these eigenstates:

$$|0\rangle = \frac{1}{\sqrt{2}}\left(|{+1}\rangle + |{-1}\rangle\right), \tag{3.14}$$

$$|1\rangle = \frac{1}{\sqrt{2}}\left(|{+1}\rangle - |{-1}\rangle\right). \tag{3.15}$$

Let us draw on Halliwell's evaluations to evolve the initial state to some t beyond t_1. This is a situation where the propagator can still take an exponential form, despite the time dependence of the Hamiltonian:

$$\begin{aligned} |\Psi(t)\rangle &= \exp\left(-\frac{i}{\hbar}\int_0^t dt'\tilde{H}(t')\right)|\Psi\rangle \\ &= \frac{1}{\sqrt{2}}\sum_{s=\pm1} e^{-iHt/\hbar}e^{-i\lambda(a+a^\dagger)\Upsilon(y)/\hbar}\,|\psi\rangle\otimes|s\rangle \\ &= \frac{1}{\sqrt{2}}\sum_{s=\pm1} e^{-iHt/\hbar}e^{-is\lambda\Upsilon(y)/\hbar}\,|\psi\rangle\otimes|s\rangle\,. \end{aligned} \tag{3.16}$$

Of course, if the particle is not within Δu, then the window function is zero valued and the end state is merely $|\Psi(t)\rangle = |\psi(t)\rangle \otimes |0\rangle$. If we are within the upper slit, then we can apply Euler's formula, reorganize terms, and find something more interesting:

$$\begin{aligned}\frac{1}{\sqrt{2}}\sum_{s=\pm 1} e^{-is\lambda/\hbar}|s\rangle &= \frac{1}{\sqrt{2}}\left[e^{-i\lambda/\hbar}|+1\rangle + e^{i\lambda/\hbar}|-1\rangle\right] \\ &= \frac{1}{\sqrt{2}}\left[\cos\left(\frac{\lambda}{\hbar}\right)|+1\rangle - i\sin\left(\frac{\lambda}{\hbar}\right)|+1\rangle + \cos\left(\frac{\lambda}{\hbar}\right)|-1\rangle + i\sin\left(\frac{\lambda}{\hbar}\right)|-1\rangle\right] \\ &= \cos\left(\frac{\lambda}{\hbar}\right)\frac{1}{\sqrt{2}}\left[|+1\rangle + |-1\rangle\right] - i\sin\left(\frac{\lambda}{\hbar}\right)\frac{1}{\sqrt{2}}\left[|+1\rangle - |-1\rangle\right] \\ &= \cos\left(\frac{\lambda}{\hbar}\right)|0\rangle - i\sin\left(\frac{\lambda}{\hbar}\right)|1\rangle\,.\end{aligned} \tag{3.17}$$

If, as I mentioned mere paragraphs ago, we go along with $\lambda = \frac{\pi\hbar}{2}$, then our time evolved final state is

$$|\Psi(t)\rangle = e^{-i(Ht/\hbar - 3\pi/2)}|\psi\rangle \otimes |1\rangle\,. \tag{3.18}$$

Note that we gain a new global phase thanks to the $-i$ factor that crops up. More germane to our earlier discussion, this Hamiltonian perfectly correlates being outside of Δu with detector state $|0\rangle$ and being inside of Δu with detector state $|1\rangle$. We can apply this to our branch wave functions for h_u and h_l:

$$|\Psi_{h_u}\rangle = -i\,|\psi_{h_u}\rangle \otimes |1\rangle\,, \tag{3.19}$$

$$|\Psi_{h_l}\rangle = |\psi_{h_l}\rangle \otimes |0\rangle\,. \tag{3.20}$$

When we evaluate the decoherence functional, we find that

$$d(h_u, h_l) = \langle\Psi_{h_l}|\Psi_{h_u}\rangle = -i\,\langle\psi_{h_l}|\psi_{h_u}\rangle\,\langle 0|1\rangle = 0. \tag{3.21}$$

Just like our abstract model, this explicit Hamiltonian leads to decoherence by creating a persistent record of which slit the particle passed through. The record nullifies the interference between alternative branches and makes our set of histories consistent.

3.3 Partial Information

Currently, our detector correlates the state $|1\rangle$ with the path going through the upper slit, and the state $|0\rangle$ with not going through the upper slit. Since there is no other way to get through the screen, that means $|0\rangle$ is perfectly correlated with going through the lower slit. In this situation, it is as though we have a device directly behind the upper slit that registers whether or not a particle passes through. When a particle strikes the detector screen, it is possible to tell whether or not it came through the upper slit, so the path information is entirely reconstructible.

Suppose we left things more general, and did not assume that $\lambda = \frac{\pi\hbar}{2}$. Then our branch wave function for h_u would be

$$|\Psi_{h_u}\rangle = |\psi_{h_u}\rangle \otimes \left[\cos\left(\frac{\lambda}{\hbar}\right)|0\rangle - i\sin\left(\frac{\lambda}{\hbar}\right)|1\rangle\right]. \tag{3.22}$$

This intermediate-seeming detector state is normalized, so it does not change the results of Eqns. 2.48 and 2.49. It does affect Eqn. 2.51, which gains a new variable factor:

$$\begin{aligned} d(h_u, h_l) &= \langle\Psi_{h_l}|\Psi_{h_u}\rangle \\ &= \langle\psi_{h_l}|\psi_{h_u}\rangle \langle 0|\left[\cos\left(\frac{\lambda}{\hbar}\right)|0\rangle - i\sin\left(\frac{\lambda}{\hbar}\right)|1\rangle\right] \\ &= \frac{m\Delta y^2}{4\pi^2\hbar 2(t_2 - t_1)}\cos\left(\frac{\lambda}{\hbar}\right) e^{i\left(\frac{p_y}{\hbar} - \frac{my_f}{\hbar(t_2-t_1)}\right)2y_0}. \end{aligned} \tag{3.23}$$

The coupling coefficient λ determines whether or not the histories decohere. If we go back to our history h_{ul} which coarse-grains the particular path out, we find that our probability density at the detector screen becomes

$$\begin{aligned} d(h_{ul}, h_{ul}) &= \frac{m\Delta y^2}{2\pi^2\hbar^2(t_2 - t_1)}\left[1 + \cos\left(\frac{\lambda}{\hbar}\right)\cos\left(\left(\frac{p_y}{\hbar} - \frac{my_f}{\hbar(t_2 - t_1)}\right)2y_0\right)\right] \\ &\approx \frac{m\Delta y^2}{2\pi^2\hbar^2(t_2 - t_1)}\left[1 + \cos\left(\frac{\lambda}{\hbar}\right)\cos\left(2\pi\frac{r_u - r_l}{\lambda_{dB}}\right)\right]. \end{aligned} \tag{3.24}$$

In the interest of quantifying the interference as it relates to the coupling coefficient, there exists a simple expression for fringe visibility [20, 22]:

$$\mathcal{V} = \frac{I_{max} - I_{min}}{I_{max} + I_{min}}. \tag{3.25}$$

Here, I_{max} indicates the greatest intensity of the interference pattern, and I_{min} indicates the lowest intensity of the interference pattern. We get the former right in the middle of the detector screen, where $r_u - r_l = 0$, which makes the second cosine take the value 1. We get our first minimum where $r_u - r_l = \frac{\lambda_{dB}}{2}$, as that would make the second cosine's argument π, and therefore the cosine itself would take the value -1. The complicated coefficient in the front is shared by all terms, so it cancels and we may evaluate rather simply:

$$\begin{aligned} \mathcal{V} &\approx \frac{\left[1 + \cos\left(\frac{\lambda}{\hbar}\right)\cos(0)\right] - \left[1 + \cos\left(\frac{\lambda}{\hbar}\right)\cos(\pi)\right]}{\left[1 + \cos\left(\frac{\lambda}{\hbar}\right)\cos(0)\right] + \left[1 + \cos\left(\frac{\lambda}{\hbar}\right)\cos(\pi)\right]} \\ &= \frac{\left[1 + \cos\left(\frac{\lambda}{\hbar}\right)\right] - \left[1 - \cos\left(\frac{\lambda}{\hbar}\right)\right]}{\left[1 + \cos\left(\frac{\lambda}{\hbar}\right)\right] + \left[1 - \cos\left(\frac{\lambda}{\hbar}\right)\right]} \\ &= \frac{2\cos\left(\frac{\lambda}{\hbar}\right)}{2} \\ &= \cos\left(\frac{\lambda}{\hbar}\right). \end{aligned} \tag{3.26}$$

Our fringe visibility varies smoothly between 1 and 0 as λ varies from 0 to $\frac{\pi\hbar}{2}$. In the case where $\lambda = 0$, $\mathcal{V} = 1$, which means we have maximum interference (because there is no coupling to the detector). When $\lambda = \frac{\pi\hbar}{2}$, $\mathcal{V} = 0$ due to our access to perfect path information.

Evaluating the situation where λ is between these two extremes does not lend itself to simple physical analogy. We have moved from a two-state detector to a detector which encodes path information in a qubit, which can be in a superposition state. In effect, we still have a particle detection device behind the upper slit, but instead of completely flipping the detector state, it places the detector into a state of quantum uncertainty. We have a chance of measuring the detector state to be $|0\rangle$ even if the particle went through the upper slit, so we have constructed an imperfect record, which leads to imperfect decoherence.

Chapter 4

Expansion Pack—Finite-Width Slits

Recall that in Section 2.3 we made an approximation (see the discussion surrounding Eqn. 2.43) to infinitely thin slits. While this was perfectly sufficient for replicating the results of purely geometrical optics, the outcome was not normalizable, having no decay as the field point on the detector screen moved away from $y = 0$.

To combat this, suppose we instead tried to make a more physically accurate model, leaving the slits with finite width. The key is to integrate Eqn. 2.37, reproduced here for your convenience:

$$\sqrt{\frac{2m\hbar}{t_2 - t_1}}\sqrt{\frac{\pi}{i}}e^{-i\frac{p_y^2}{2m}(t_2-t_1)/\hbar}e^{ip_y y_f/\hbar}\int_{y_0-\frac{\Delta y}{2}}^{y_0+\frac{\Delta y}{2}} dy \exp\left(i\left[\sqrt{\frac{m}{2\hbar(t_2-t_1)}}y + \frac{1}{2}\sqrt{\frac{2\hbar(t_2-t_1)}{m}}\left(\frac{p_y}{\hbar} - \frac{my_f}{\hbar(t_2-t_1)}\right)\right]^2\right). \tag{2.37}$$

This integral is the result of evolving the plane wave projected onto the upper slit forward in time, then projecting onto the detector screen. One tactic attempted was to apply the substitution given in Eqn. 2.38:

$$y' = \sqrt{\frac{m}{2\hbar(t_2-t_1)}}y + \frac{1}{2}\sqrt{\frac{2\hbar(t_2-t_1)}{m}}\left(\frac{p_y}{\hbar} - \frac{my_f}{\hbar(t_2-t_1)}\right) \implies dy' = \sqrt{\frac{m}{2\hbar(t_2-t_1)}}dy. \tag{2.38}$$

That allowed us to morph Eqn. 2.37 into Eqn. 2.39:

$$2\hbar\sqrt{\frac{\pi}{i}}e^{-i\frac{p_y^2}{2m}(t_2-t_1)/\hbar}e^{ip_y y_f/\hbar}\int_{\Delta u'} dy' \exp\left(iy'^2\right). \tag{2.39}$$

However, this is still difficult to work with. It almost looks like a Gaussian integral, which we know how to evaluate, but the argument of the exponent lacks a negative sign, and the bounds of integration do not stretch from $-\infty$ to ∞. Our original solution tactic (Eqn. 2.31) cannot be applied. Once we employ some new tricks, we will have new, better expressions for our branch wave functions, and can see a more interesting probability density than a simple sinusoidal expression.

4.1 It Runs On Imagination

Going forward, we will want to make use of the imaginary error function [23]

$$\text{erfi}(z) = \frac{\text{erf}(iz)}{i}. \tag{4.1}$$

The error function is built on the integral of a Gaussian:

$$\text{erf}(z) = \frac{2}{\sqrt{\pi}} \int_0^z dt e^{-t^2}. \tag{4.2}$$

This means that the imaginary error function is

$$\text{erfi}(z) = \frac{2}{i\sqrt{\pi}} \int_0^{iz} dt e^{-t^2}, \tag{4.3}$$

and we can manipulate this with the substitution $it' = t$ ($\implies idt' = dt$):

$$\text{erfi}(z) = \frac{2}{\sqrt{\pi}} \int_0^z dt' e^{t'^2}. \tag{4.4}$$

This is close to what we want, since we have eliminated the negative sign. More specifically, we are going to need to know the integral of e^{it^2}. This is a special case of integrating e^{at^2}, where a is some constant. If we begin with $\text{erfi}(\sqrt{a}z)$ and make the substitution $\sqrt{a}t = t'$, we can reach the desired integral:

$$\begin{aligned} \text{erfi}(\sqrt{a}z) &= \frac{2}{\sqrt{\pi}} \int_0^{\sqrt{a}z} dt' e^{t'^2} \\ &\qquad \sqrt{a}t = t' \implies \sqrt{a}dt = dt' \\ &= 2\sqrt{\frac{a}{\pi}} \int_0^z dt e^{at^2}. \end{aligned} \tag{4.5}$$

Now we can let $a = i$ to get

$$\text{erfi}(\sqrt{i}z) = 2\sqrt{\frac{i}{\pi}} \int_0^z e^{it^2}, \tag{4.6}$$

which means we can solve an integral of e^{it^2} involving a nonzero lower bound:

$$\int_{z_0}^{z_1} dt e^{it^2} = \frac{1}{2}\sqrt{\frac{\pi}{i}} \left[\text{erfi}(\sqrt{i}z_1) - \text{erfi}(\sqrt{i}z_0)\right]. \tag{4.7}$$

This is exactly what we needed to solve Eqn. 2.39!

4.2 Revising Histories

What remains is to figure out what the bounds of integration are, given the substitution used (Eqn. 2.38). The original region of integration (Eqn. 2.3) had lower bound $y_0 - \frac{\Delta y}{2}$ and upper bound $y_0 + \frac{\Delta y}{2}$, so the new region of integration will be

$$\begin{aligned} \Delta u' = \Bigg[&\sqrt{\frac{m}{2\hbar(t_2 - t_1)}} \left(y_0 - \frac{\Delta y}{2}\right) + \frac{1}{2}\sqrt{\frac{2\hbar(t_2 - t_1)}{m}} \left(\frac{p_y}{\hbar} - \frac{m y_f}{\hbar(t_2 - t_1)}\right), \\ &\sqrt{\frac{m}{2\hbar(t_2 - t_1)}} \left(y_0 + \frac{\Delta y}{2}\right) + \frac{1}{2}\sqrt{\frac{2\hbar(t_2 - t_1)}{m}} \left(\frac{p_y}{\hbar} - \frac{m y_f}{\hbar(t_2 - t_1)}\right) \Bigg]. \end{aligned} \tag{4.8}$$

This expression can be simplified, however:

$$\begin{aligned}\Delta u' = \Bigg[&\sqrt{\frac{m}{2\hbar(t_2-t_1)}}\left(y_0 - \frac{\Delta y}{2} - y_f\right) + \sqrt{\frac{t_2-t_1}{2m\hbar}}p_y, \\ &\sqrt{\frac{m}{2\hbar(t_2-t_1)}}\left(y_0 + \frac{\Delta y}{2} - y_f\right) + \sqrt{\frac{t_2-t_1}{2m\hbar}}p_y\Bigg].\end{aligned} \tag{4.9}$$

As in the discussion preceding Eqn. 2.59, we want to set $p_y = 0$, because most double-slit experiments do not involve incoming particles with significant momentum parallel to the screen. In Section 2.3, we waited until late in the game to make this change, but for the following calculations, we will want to remove p_y to make room now. With this determined, Eqn. 2.39 becomes

$$\begin{aligned}&2\hbar\sqrt{\frac{\pi}{i}}e^{-i\frac{0^2}{2m}(t_2-t_1)/\hbar}e^{i(0)y_f/\hbar}\int_{\sqrt{\frac{m}{2\hbar(t_2-t_1)}}\left(y_0-\frac{\Delta y}{2}-y_f\right)}^{\sqrt{\frac{m}{2\hbar(t_2-t_1)}}\left(y_0+\frac{\Delta y}{2}-y_f\right)} dy' \exp\left(iy'^2\right) = \\ &-i\pi\hbar\left\{\text{erfi}\left[\sqrt{\frac{im}{2\hbar(t_2-t_1)}}\left(y_0+\frac{\Delta y}{2}-y_f\right)\right] - \text{erfi}\left[\sqrt{\frac{im}{2\hbar(t_2-t_1)}}\left(y_0-\frac{\Delta y}{2}-y_f\right)\right]\right\}.\end{aligned} \tag{4.10}$$

This goes into Eqn. 2.28 where the double integral is, giving us the upper branch wave function

$$\begin{aligned}|\psi_{h_u}\rangle = U(t_0,t_2)\Bigg(\frac{-i}{2\sqrt{2\pi\hbar}}e^{-i\frac{p_x^2}{2m}(t_2-t_0)/\hbar}\Bigg\{&\text{erfi}\left[\sqrt{\frac{im}{2\hbar(t_2-t_1)}}\left(y_0+\frac{\Delta y}{2}-y_f\right)\right] \\ &-\text{erfi}\left[\sqrt{\frac{im}{2\hbar(t_2-t_1)}}\left(y_0-\frac{\Delta y}{2}-y_f\right)\right]\Bigg\}\Bigg)|p_x\rangle\otimes|y_f\rangle.\end{aligned} \tag{4.11}$$

Naturally, it is not all that much of a substitution to find the lower branch wave function as well:

$$\begin{aligned}|\psi_{h_l}\rangle = U(t_0,t_2)\Bigg(\frac{-i}{2\sqrt{2\pi\hbar}}e^{-i\frac{p_x^2}{2m}(t_2-t_0)/\hbar}\Bigg\{&\text{erfi}\left[\sqrt{\frac{im}{2\hbar(t_2-t_1)}}\left(-y_0+\frac{\Delta y}{2}-y_f\right)\right] \\ &-\text{erfi}\left[\sqrt{\frac{im}{2\hbar(t_2-t_1)}}\left(-y_0-\frac{\Delta y}{2}-y_f\right)\right]\Bigg\}\Bigg)|p_x\rangle\otimes|y_f\rangle.\end{aligned} \tag{4.12}$$

With these new histories, we now see that their decoherence functionals with themselves are no longer constant:

$$\begin{aligned}d(h_u,h_u) &= \langle\psi_{h_u}|\psi_{h_u}\rangle \\ &= \frac{1}{8\pi\hbar}\left\{\text{erfi}\left[\sqrt{\frac{im}{2\hbar(t_2-t_1)}}\left(y_0+\frac{\Delta y}{2}-y_f\right)\right] - \text{erfi}\left[\sqrt{\frac{im}{2\hbar(t_2-t_1)}}\left(y_0-\frac{\Delta y}{2}-y_f\right)\right]\right\}^* \\ &\quad\times\left\{\text{erfi}\left[\sqrt{\frac{im}{2\hbar(t_2-t_1)}}\left(y_0+\frac{\Delta y}{2}-y_f\right)\right] - \text{erfi}\left[\sqrt{\frac{im}{2\hbar(t_2-t_1)}}\left(y_0-\frac{\Delta y}{2}-y_f\right)\right]\right\},\end{aligned} \tag{4.13}$$

$$\begin{aligned}d(h_l,h_l) &= \langle\psi_{h_l}|\psi_{h_l}\rangle \\ &= \frac{1}{8\pi\hbar}\left\{\text{erfi}\left[\sqrt{\frac{im}{2\hbar(t_2-t_1)}}\left(-y_0+\frac{\Delta y}{2}-y_f\right)\right] - \text{erfi}\left[\sqrt{\frac{im}{2\hbar(t_2-t_1)}}\left(-y_0-\frac{\Delta y}{2}-y_f\right)\right]\right\}^* \\ &\quad\times\left\{\text{erfi}\left[\sqrt{\frac{im}{2\hbar(t_2-t_1)}}\left(-y_0+\frac{\Delta y}{2}-y_f\right)\right] - \text{erfi}\left[\sqrt{\frac{im}{2\hbar(t_2-t_1)}}\left(-y_0-\frac{\Delta y}{2}-y_f\right)\right]\right\}.\end{aligned} \tag{4.14}$$

These do not replicate any solution form that has been presented thus far. Let us graph Eqn. 4.13 and examine its shape.

Suppose we send an electron (approximated as $m \approx 9.1 \times 10^{-31}$ kg [1]) at $v = 1100$ m/s toward a single slit at height $y_0 = 0$ m. This mass and velocity correspond to a momentum $p_x \approx 10^{-27}$ kg·m/s, which means the electron has a deBroglie wavelength of $\lambda_{dB} = \frac{h}{p_x} \approx 6.63 \times 10^{-7}$ m (where we take $h \approx 6.626 \times 10^{-34}$ J·s), which corresponds to the wavelength of light on the red end of the visible spectrum [15]. We position the detector screen 1.1 m past the slit, which gives us a convenient $t_2 - t_1 = 10^{-3}$ s for the electron to travel from the slit to the screen. We are no longer required to use an incredibly thin slit to comply with an approximation, so we can take a more standard width of $\Delta y = 10^{-4}$ m [15]. This situation is graphed in Fig. 4.1, albeit with $d(h_u, h_u)$ multiplied by $800\pi\hbar$ to keep the vertical scale down ($1/\hbar$ is very large, after all).

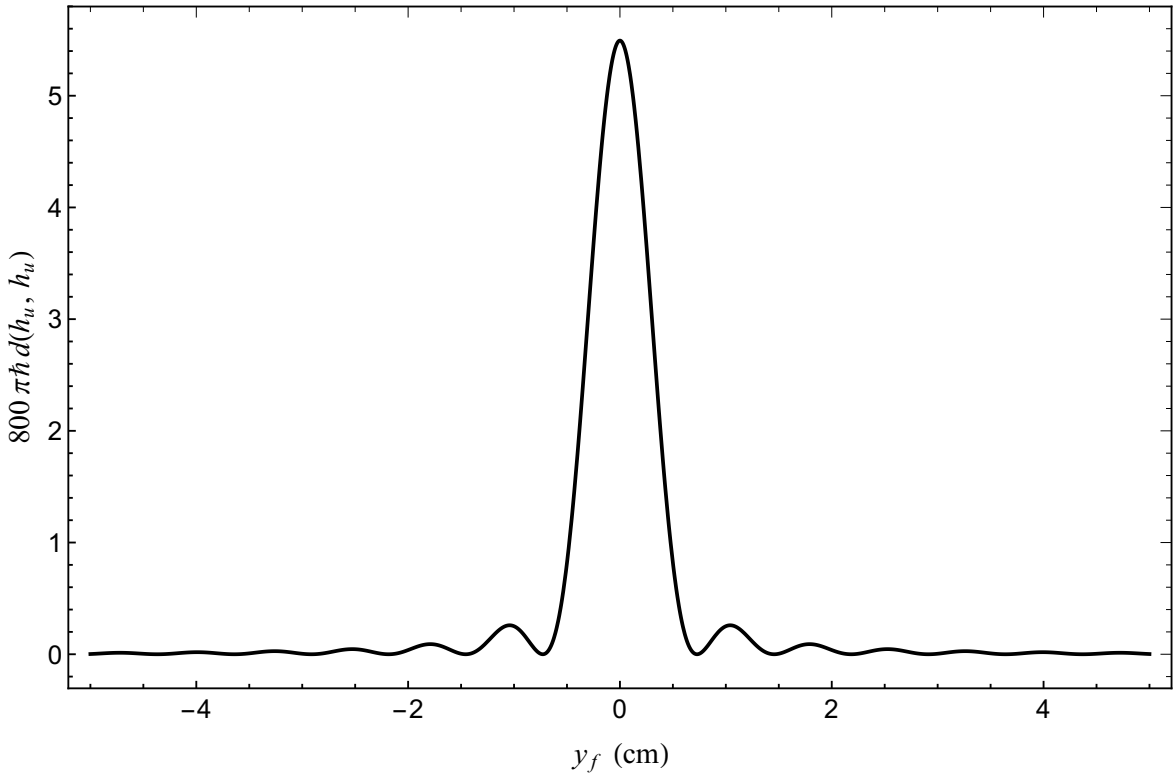

Figure 4.1: Single-Slit Diffraction A bright central fringe in the interference pattern is characteristic of single-slit diffraction [15]. The plotted curve of $800\pi\hbar d(h_u, h_u)$ uses values $y_0 = 0$ m, $\Delta y = 10^{-4}$ m, $m = 9.1 \times 10^{-31}$ kg, and $t_2 - t_1 = 10^{-3}$ s. The code used to generate this plot can be found in Section A.1.

As we can see in Fig. 4.1, the magnitude of the probability density decays very rapidly away from the center, as opposed to the behavior of Eqn. 2.60, which simply oscillates across the detector screen without necessarily vanishing to zero. Figure 4.1 depicts the phenomenon of single-slit diffraction, reproduced by the mathematics of the consistent histories formalism.

Let us graduate back up to two slits. We will need the decoherence functional comparing h_u with h_l:

$$d(h_u,h_l) = \langle\psi_{h_l}|\psi_{h_u}\rangle = \frac{1}{8\pi\hbar}\left\{\text{erfi}\left[\sqrt{\frac{im}{2\hbar(t_2-t_1)}}\left(-y_0+\frac{\Delta y}{2}-y_f\right)\right]-\text{erfi}\left[\sqrt{\frac{im}{2\hbar(t_2-t_1)}}\left(-y_0-\frac{\Delta y}{2}-y_f\right)\right]\right\}^* \times\left\{\text{erfi}\left[\sqrt{\frac{im}{2\hbar(t_2-t_1)}}\left(y_0+\frac{\Delta y}{2}-y_f\right)\right]-\text{erfi}\left[\sqrt{\frac{im}{2\hbar(t_2-t_1)}}\left(y_0-\frac{\Delta y}{2}-y_f\right)\right]\right\}. \tag{4.15}$$

Now, being less approximate doesn't change the fact that $\{h_u, h_l\}$ is not a consistent set, so we need to consider the coarse grained history from Eq. 2.52. Let us also recall the punchline from Eqn. 2.53:

$$d(h_{ul},h_{ul}) = \langle\psi_{h_u}|\psi_{h_u}\rangle + \langle\psi_{h_u}|\psi_{h_l}\rangle + \langle\psi_{h_l}|\psi_{h_u}\rangle + \langle\psi_{h_l}|\psi_{h_l}\rangle\,.$$

We know that $\langle\psi_{h_u}|\psi_{h_l}\rangle$ and $\langle\psi_{h_l}|\psi_{h_u}\rangle$ are complex conjugates of each other, so their sum is merely twice the real component of either one. This allows us to massage our result into a better form:

$$\begin{aligned} d(h_{ul},h_{ul}) &= \langle\psi_{h_u}|\psi_{h_u}\rangle + \langle\psi_{h_l}|\psi_{h_l}\rangle + 2\Re\left[\langle\psi_{h_l}|\psi_{h_u}\rangle\right] \\ &= d(h_u,h_u) + d(h_l,h_l) + 2\Re\left[d(h_u,h_l)\right]. \end{aligned} \tag{4.16}$$

This is the probability density for our double-slit interference pattern. I will not be inserting Eqns. 4.13, 4.14, or 4.15, simply because they are far too large, and the expression would be a terrible, pointless mess.

If we were to include a variable-accuracy path detector, as in Section 3.3, we know that a factor of $\cos\left(\frac{\lambda}{\hbar}\right)$ would emerge as part of $d(h_u,h_l)$ under the Hamiltonian from Eqn. 3.11. Rather than redefine Eqn. 4.15 to include this coupling-dependent factor, we can place a cosine factor in front of the interference term, making our full interference pattern expression

$$d(h_{ul},h_{ul}) = d(h_u,h_u) + d(h_l,h_l) + 2\cos\left(\frac{\lambda}{\hbar}\right)\Re\left[d(h_u,h_l)\right]. \tag{4.17}$$

Technically, I am being notationally sloppy again, but sticking the cosine in separately keeps the machinery from being too hidden.

To obtain probabilities for a double slit, we now need a slit spacing, which for us is actually $2y_0$. A reasonable spacing would be 0.5 mm [15], which means $y_0 = 2.5$ mm. Figures 4.2, 4.3, and 4.4 depict a most fascinating transition from maximal interference and no path information (Fig. 4.2a) to perfect path information and no interference (Fig. 4.4b).

These serve to illustrate what Eqn. 3.26 was getting at: a smooth transition through levels of partial path information, from wave behavior to particle behavior. This is the essence of the mystery inherent in the double-slit experiment, that we can see—and now I can emphasize *see*—the mixture of these two classically incompatible behaviors.

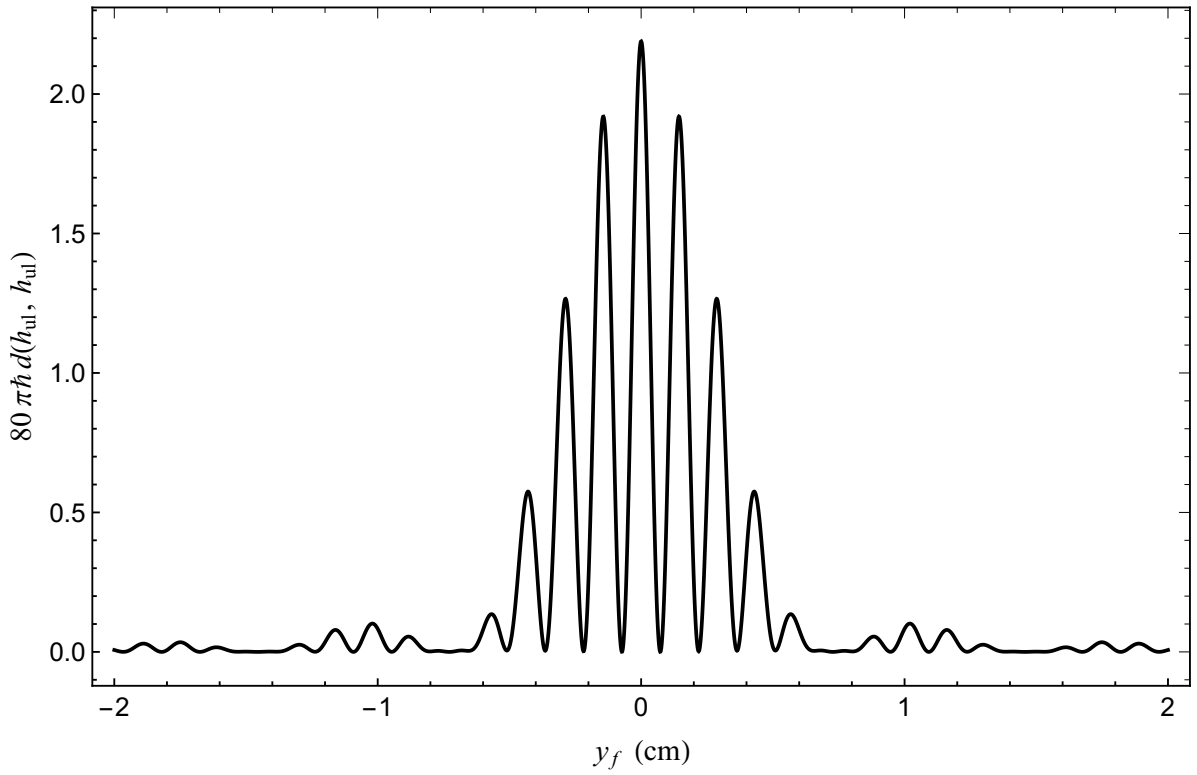

(a) $\lambda = 0$

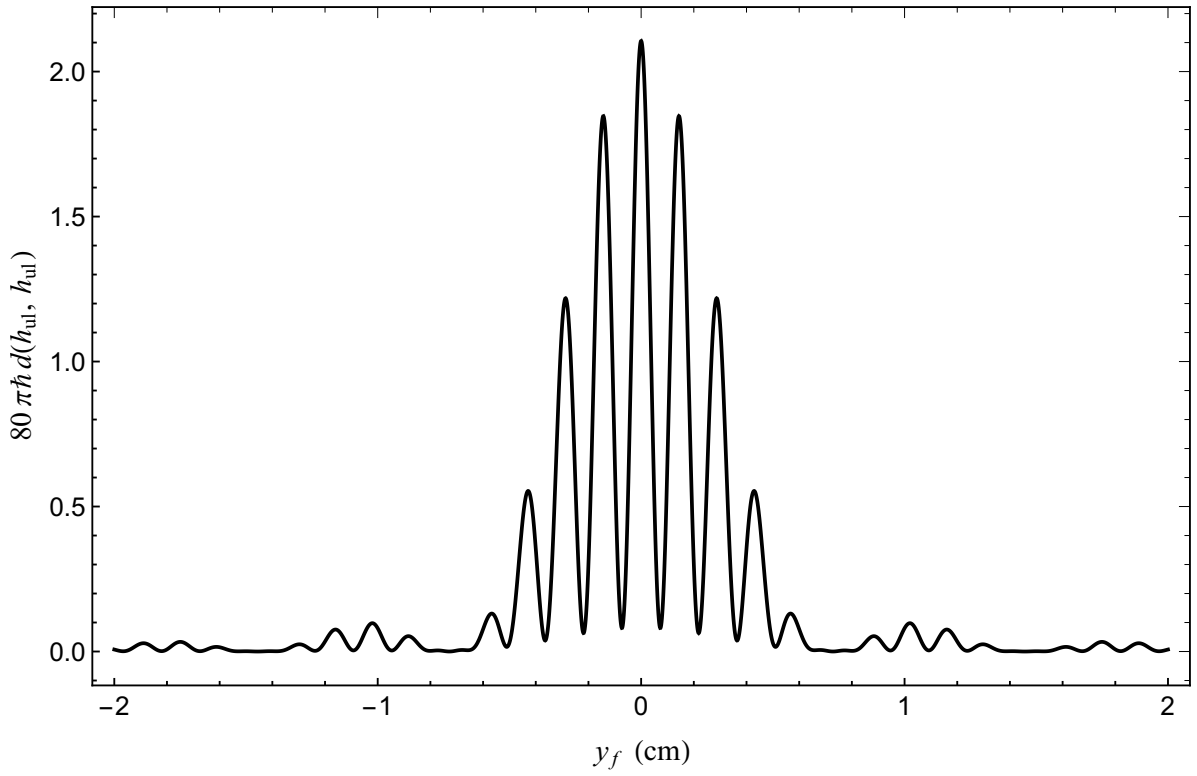

(b) $\lambda = \frac{\pi\hbar}{8}$

Figure 4.2: Double-Slit Diffraction with $\lambda = 0$ and $\lambda = \frac{\pi\hbar}{8}$ In plot (a), we see the interference fringes of a system with no path information. When we introduce an imperfect path detector in plot (b), there is a slight change in the pattern, with the minima eking up and the maxima lowering slightly. The plotted curves of $80\pi\hbar d(h_u, h_u)$ use values $y_0 = 2.5 \times 10^{-4}$ m, $\Delta y = 10^{-4}$ m, $m = 9.1 \times 10^{-31}$ kg, and $t_2 - t_1 = 10^{-3}$ s. The code used to generate these plots can be found in Section A.2.

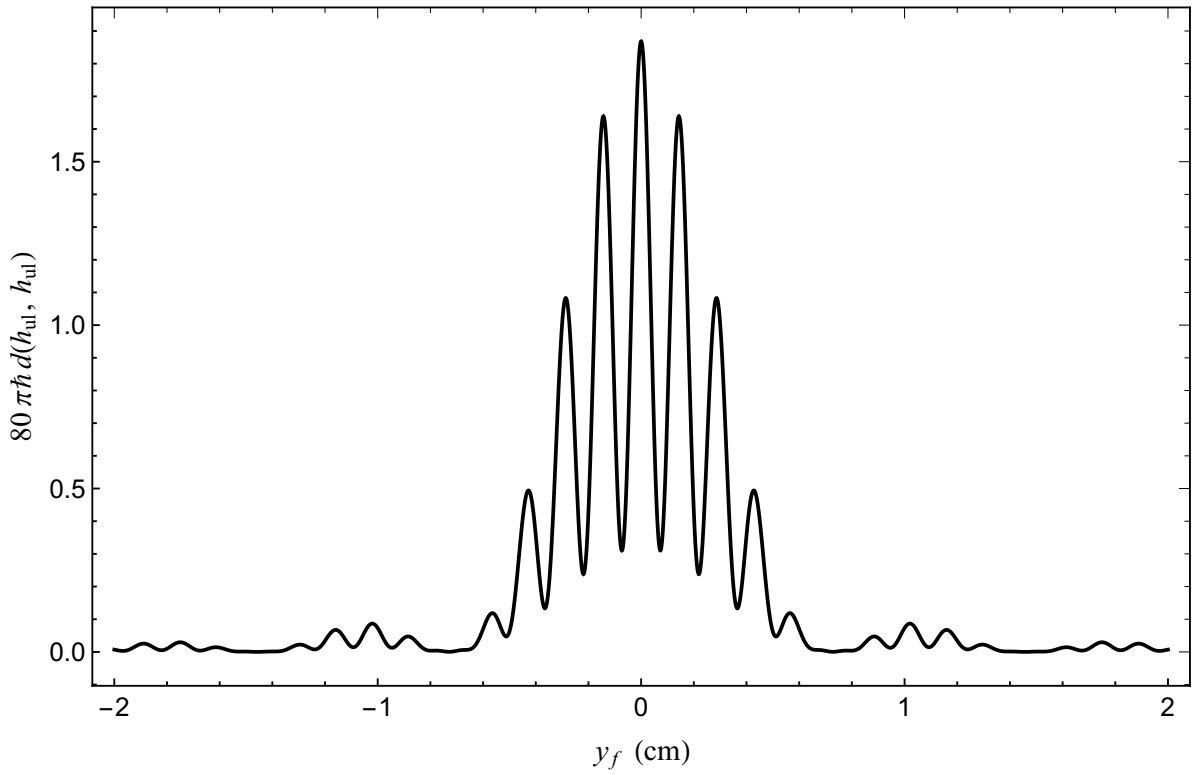

(a) $\lambda = \frac{\pi\hbar}{4}$

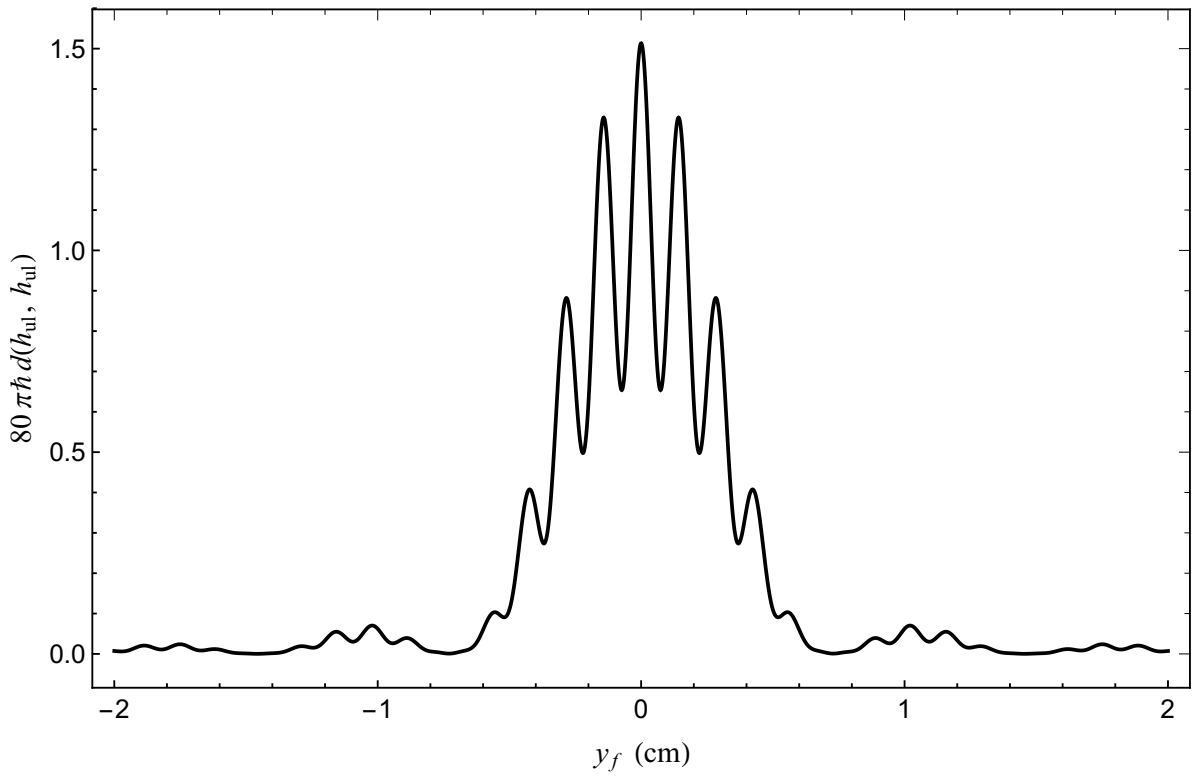

(b) $\lambda = \frac{3\pi\hbar}{8}$

Figure 4.3: Double-Slit Diffraction with $\lambda = \frac{\pi\hbar}{4}$ and $\lambda = \frac{3\pi\hbar}{8}$ In plot (a), the increasing quality of the record has noticeably deformed the pattern. The effect is even more pronounced in plot (b). The slow vanishing of interference as the detector improves is becoming clear. The plotted curves of $80\pi\hbar d(h_u, h_u)$ use values $y_0 = 2.5 \times 10^{-4}$ m, $\Delta y = 10^{-4}$ m, $m = 9.1 \times 10^{-31}$ kg, and $t_2 - t_1 = 10^{-3}$ s. The code used to generate these plots can be found in Section A.2.

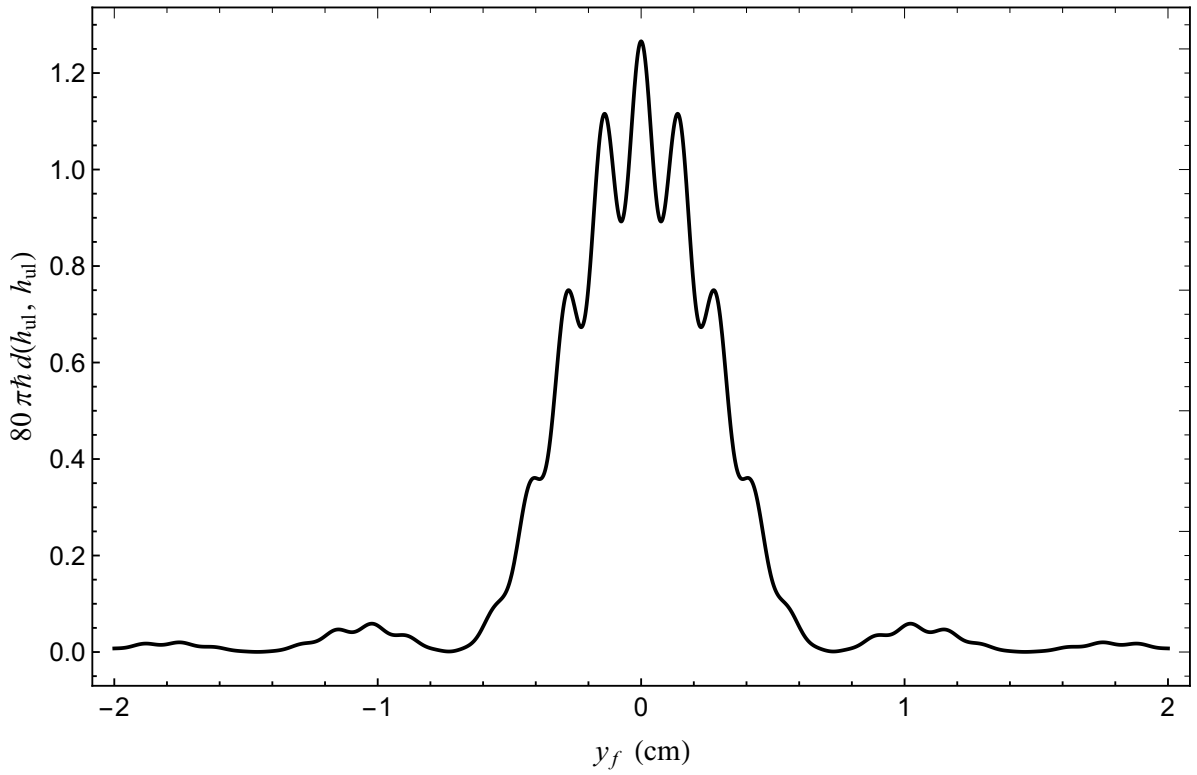

(a) $\lambda = \frac{9\pi\hbar}{20}$

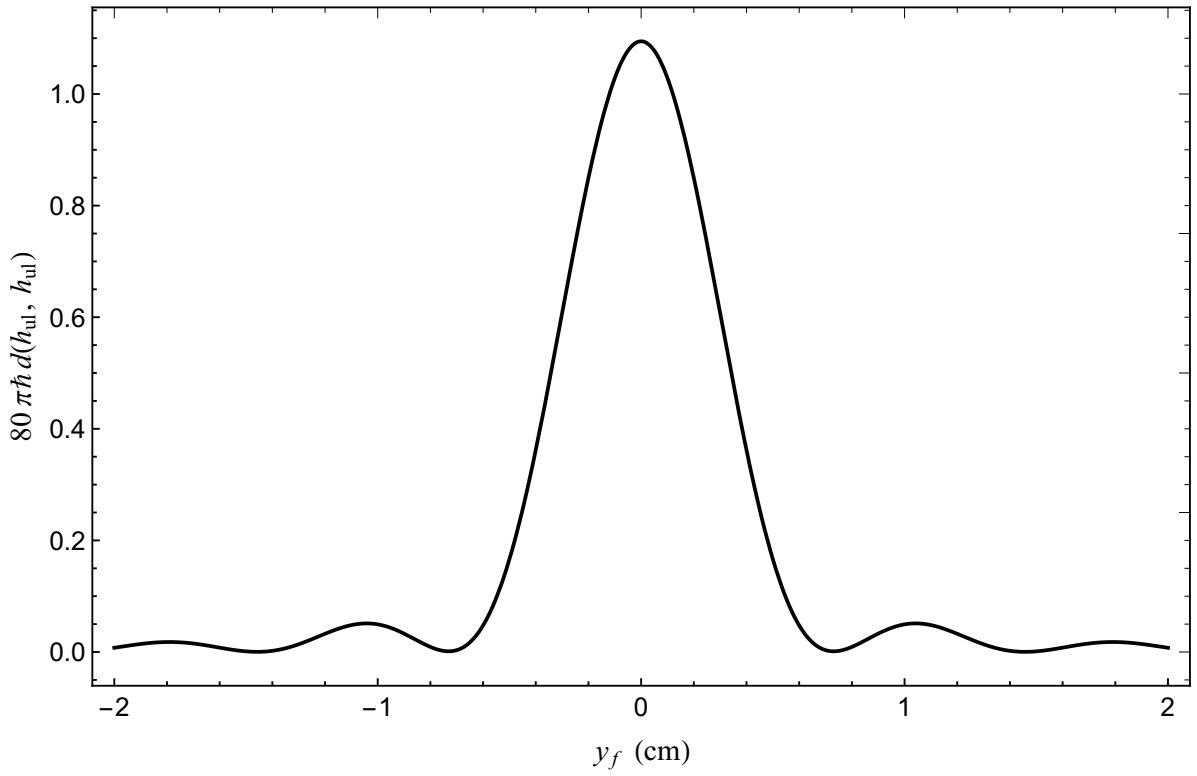

(b) $\lambda = \frac{\pi\hbar}{2}$

Figure 4.4: Double-Slit Diffraction with $\lambda = \frac{9\pi\hbar}{20}$ and $\lambda = \frac{\pi\hbar}{2}$ Plot (a) shows only the barest hints of interference, as the detector is recording nearly perfect path information. Once we adjust the coupling coefficient to the optimal value in plot (b), we have perfect path information, removing all interference. This pattern is consistent with particle behavior, traversing only one slit at a time, though the slits are so close on this scale that their diffraction patterns overlap almost perfectly. The plotted curves of $80\pi\hbar d(h_u, h_u)$ use values $y_0 = 2.5 \times 10^{-4}$ m, $\Delta y = 10^{-4}$ m, $m = 9.1 \times 10^{-31}$ kg, and $t_2 - t_1 = 10^{-3}$ s. The code used to generate these plots can be found in Section A.2.

Chapter 5

Dénouement

We set out on this journey together with one goal explicitly stated: to develop an example of applying the consistent histories formalism in order to assist others in understanding it. It turns out that we have gained fascinating insights into the double-slit experiment as well. Now, in the clearing at the end of the path, let us extract the fruits of our labor and set them out to be given their due.

5.1 Following the Trail of Breadcrumbs

Some day, you may find yourself engaging with the quantum world on paper, on a computer, or maybe on some sort of monochromatic board, and for whatever reason, the Copenhagen interpretation will not cut it. Perhaps all you will want is to look at the problem with a fresh perspective, in case some quirk of the situation is more apparent formulated in terms of consistent histories. On the other hand, perhaps taking a more generalized approach is mandated by the nature of your work; you may be working with a closed system, trying to assign probabilities to sequences of events that go without direct observation. Whatever the case, the consistent histories formalism is there for you, and you have seen it in action.

With the parameters of your system defined in sufficient detail, start determining all of the different sequences of events that could take place. For the double-slit experiment, this consisted of the particle traveling through the upper slit to the detector screen, and the particle traveling through the lower slit to the detector screen.

Once you have your set of histories in hand, begin to compare them to each other. If any pair of histories is not orthogonal, then the set is not consistent. This means that you will have to coarse-grain some events, merging alternatives to create less specific chains of events. In the double-slit experiment, we had to remove the distinction between going through one slit or the other, creating a new history where the particule could reach its destination without its path being determined in classically sensible terms.

Alternatively, consistency can be achieved by introducing more elements to the system to force the set

to decohere. This was the point of Chapter 3, where we added a detector to record the slit the particle went through. With the path information stored and persistent, the original two histories became orthogonal, and the set became consistent.

Whichever method is applied, the consistent set of histories can be evaluated to determine the probability of each particular sequence of events. The math to get all the way here may not be simple (remember Eqn. 2.29), but application of the formalism itself is straightforward, once you get the hang of it.

Learning only by being told how to do something can be challenging. Even the clearest description of a process used on an abstract case may not be sufficient to make things click. Oftentimes, a specific case and all of its details must be seen to truly get one's mind ready for the task of applying a new method. For those who need it, my work has been laid bare in the hope that your how-to questions about the consistent histories formalism will be answered. If your endeavor to learn and use the formalism for your own purposes is facilitated in any way, then my efforts will have been worthwhile.

5.2 Two Slits Diverged

Beyond whatever aid I may have provided, we have seen Young's experiment in a different light than we often do, and there are certainly things worth noting in the aftermath.

To begin, you may have reached the end of Chapter 2 and thought, "Big whoop. We got this result from geometric optics already." In all honesty, Chapter 2 was especially educationally focused, and does reinvent the wheel, in a sense. However, sometimes you can learn more about wheels by building them than by using them. The optics perspective deals in the interference of waves, but we have dealt in the interference of alternatives. We have seen not only that passing through the slits in a nonspecific, wavelike manner leads to interference fringes at the detector screen, but passing through one slit or the other leads to a meaningless description of the system. If we take the probability density of the particle transiting the upper slit and reaching a point on the detector screen, and add it to the probability density of the particle transiting the lower slit and reaching the same point, we find that they do not sum to the actual total probability of the particle arriving at that final position. There are no valid probabilities for taking one path versus the other without some sort of path detector making the events distinguishable after the fact.

This was the idea explored in Chapter 3. We tied a direct line between the transition to particle behavior and the existence of an unambiguous record of events. The ability to access information about the path of the particle led to it going through one slit or the other, as a classical particle should. This serves a dual purpose, illustrating both an original point about the power of the formalism and also underscoring the paradox of the double-slit experiment.

Regarding the formalism, one of my earliest remarks concerned how we do not require classical observers

making measurements to determine a system's outcomes and probabilities. All we did in Section 3.2 was attach a free bit of information to the initial state and determine its interaction with the system. Without appealing to the outside world, we made the interference go away; we treated the double-slit experiment as a closed system, and that little record inside was all that was needed to make particle behavior emerge. No one had to peek over the system's shoulder to get the job done.

We were really playing around with that record when we got to Section 3.3. By tweaking the distinguishability of the final detector states, we could make the interference fringes vanish smoothly. At one end of the spectrum is strict wave behavior, and at the other is strict particle behavior. By fine-tuning the quality of the record, we can catch the system *in between* the two. The quanton behaves as a mixture of particle and wave, two classically distinct concepts. That is what makes the quantum realm so different, and what makes the double-slit experiment such an integral part of our inquiries into the quantum world.

This particle behavior I keep mentioning can be seen to reach a limit in Chapter 4, where we make the slits wide. Single-slit diffraction, a phenomenon inherent to waves, is seen to occur, either alone when only one slit is traversable (Fig. 4.1), or overlaid with an interference pattern when both are open and unobserved (Fig. 4.2a). Even with a path detector in play (Fig. 4.4b), only double-slit interference goes away, leaving single-slit patterns behind. Even this can be considered partial particle behavior. Sure, the quanton only travels through one slit or the other, but it diffracts like a wave through the one it passes through. This is because our detector is not so fine that it determines the pinpoint position of the quanton; all it does is distinguish between the two slits. Even if the detector did nail down the quanton to one spot, there is no mechanism to keep its location exactly determined in the space between the two screens, allowing it to spread out once again. Classical particle behavior becomes more finely determined as more information is recorded about the system. Imagine the amount of information that must be dispersed into the world every day to keep the majority of our experience in the classical realm. The double-slit experiment paints an even more expansive picture than one might originally think, does it not?

5.3 Further Musings

Of course, there are still questions to be answered about the double-slit experiment as expressed through the lens of consistent histories. For one thing, before the inclusion of path detection, while we are firmly in the realm of wave behavior, we are lacking decay with distance. Sure, we see that the probability densities in Figures 4.1 and 4.2a taper off as y approaches $\pm\infty$, but that is an interference effect from single slit diffraction [15]. Putting that aside, we know that a wave spreading out in space must carry the same amount of energy over a wider and wider area, causing a decay in the intensity across the wave front. This sort of effect does not emerge from the math I have done.

Before going through the trouble of evaluating finite-width slits, I had hoped to include decay in the results of Section 2.3. No trick I played seemed sufficient to evoke the desired behavior, and no resource I explored seemed to help me understand what was missing. In fact, a paper I found by Bardou simply implemented spherical decay of waves from point sources at the outset, treating it as completely given [24]. Unraveling the mystery of getting decay from the math would be very enlightening with regard to the finer points of implementing the consistent histories formalism.

One possible avenue of inquiry has to do with the physical picture painted by the initial condition and the projections applied to them. Specifically, we always talk about the experiment in terms of a particle or a light beam traveling to the slit, but that is not what we described when we set $|\psi\rangle = |p\rangle$. Recall Eqn. 2.1:

$$\langle \vec{x}|\vec{p}\rangle = \frac{1}{\sqrt{2\pi\hbar}} e^{i\vec{p}\cdot\vec{x}/\hbar}. \tag{2.1}$$

Looking at a general plane wave in the position basis, it is clear to see that it is defined across all of space. We can insert any value of $\vec{x}$, and the function has a definite value at that point. This doesn't describe an approaching particle, but a static wave over the entire plane.

Furthermore, the projector $\tilde{P}^y_{\Delta u}$ acts across all of space, not just at a particular location. This leads to our state at t_1 being truncated in regions where $y \notin \Delta u$; the new shape is still defined for all $x \in (-\infty, \infty)$, but the projector has left it nonzero only in a band of width Δy centered at y_0. This is conceptually depicted in Fig. 5.1.

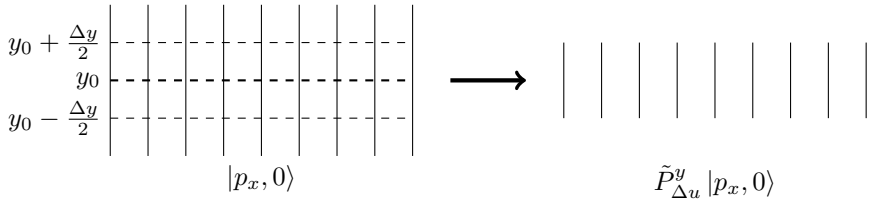

Figure 5.1: Truncated Wave A wave traveling to the right is projected onto $\left[y_0 - \frac{\Delta y}{2}, y_0 + \frac{\Delta y}{2}\right]$, which crops off all parts of the plane beyond that region. As indicated by the notation below the illustration, this is analogous to the plane wave $|p_x, 0\rangle$ being acted upon by the projector $\tilde{P}^y_{\Delta u}$. Though it is not possible to draw, the wave extends infinitely across the horizontal axis, before and after the projection event.

The next step in our history is to evolve this band over the time it takes to travel from the slit to the detector screen—except it is already defined at the screen. That is an interesting little brain teaser, isn't it? What situation are we describing with our history, exactly? Perhaps it is equivalent to the description of a steady state, as though we are training a constant laser beam upon the slit, instead of firing a particle or a pulse. That is speculation, however, deserving more careful examination. It would be interesting to see how the result would (or perhaps would not) differ if a traveling wave packet were used as the initial state. It may be that a refinement of the system could help with the decay issue as well, but I cannot say for certain.

Alas, time and defense schedules wait for no man, and I cannot provide all of the answers in this document. Mayhap I will riddle these matters out in the future, but until then, Gentle Reader, I hope what I have accomplished serves you well. Perhaps these unanswered questions will find a better home in your hands. Until next time, and ...

In case I don't see you,
Good afternoon, good evening, and good night.

—from *The Truman Show*

Appendix A

Mathematica Code

To generate the Mathematica plots used in Chapter 4, one must first set the following variables:

```
m = 9.1*10^-31;
\[HBar] = 6.626*10^-34/(2 \[Pi]);
dely = 10^-4;
y0 = 5*10^-4;
delt = 10^-3;
```

A.1 Single-Slit Diffraction

We begin by defining a function based on Eqn. 4.13, albeit without the leading constant:

```
SSD[y_] :=
Conjugate[(Erfi[Sqrt[(I m)/(2 \[HBar] delt)] (dely/2 - y)] -
Erfi[Sqrt[(I m)/(2 \[HBar] delt)] (-(dely/2) - y)])]*(Erfi[
Sqrt[(I m)/(2 \[HBar] delt)] (dely/2 - y)] -
Erfi[Sqrt[(I m)/(2 \[HBar] delt)] (-(dely/2) - y)])
```

With that done, the code for Fig. 4.1 is

```
Plot[100*SSD[y/100], {y, -5, 5}, PlotRange -> Full, Frame -> True,
FrameStyle -> Directive[Black], Axes -> False,
FrameLabel -> {Style["\!\(\*SubscriptBox[\(y\), \(f\)]\)  (cm)",
Plain, 16, FontFamily -> "Times New Roman"],
Style[ToExpression["800 \\pi \\hslash d(h_{u},h_{u})", TeXForm],
Plain, 16, FontFamily -> "Times New Roman"]},
FrameTicksStyle -> Larger, PlotStyle -> {Black, Thick}]
```

A.2 Double-Slit Interference

First, we define a function based on 4.17, again without the leading constant of Eqns. 4.13, 4.14, and 4.15:

```
DSD[y_, \[Lambda]_] :=
Conjugate[(Erfi[Sqrt[(I m)/(2 \[HBar] delt)] (y0 + dely/2 - y)] -
Erfi[Sqrt[(I m)/(2 \[HBar] delt)] (y0 - dely/2 - y)])]*(Erfi[
Sqrt[(I m)/(2 \[HBar] delt)] (y0 + dely/2 - y)] -
Erfi[Sqrt[(I m)/(2 \[HBar] delt)] (y0 - dely/2 - y)]) +
Conjugate[(Erfi[Sqrt[(I m)/(2 \[HBar] delt)] (-y0 + dely/2 - y)] -
Erfi[Sqrt[(I m)/(2 \[HBar] delt)] (-y0 - dely/2 - y)])]*(Erfi[
Sqrt[(I m)/(2 \[HBar] delt)] (-y0 + dely/2 - y)] -
Erfi[Sqrt[(I m)/(2 \[HBar] delt)] (-y0 - dely/2 - y)]) +
2 Cos[\[Pi]/2 \[Lambda]] Re[
Conjugate[(Erfi[Sqrt[(I m)/(2 \[HBar] delt)] (-y0 + dely/2 - y)] -
Erfi[Sqrt[(I m)/(
2 \[HBar] delt)] (-y0 - dely/2 - y)])]*(Erfi[
Sqrt[(I m)/(2 \[HBar] delt)] (y0 + dely/2 - y)] -
Erfi[Sqrt[(I m)/(2 \[HBar] delt)] (y0 - dely/2 - y)])]
```

The factor λ used here is not quite the coupling coefficient of Eqn. 3.11, as I removed the factor of $1/\hbar$ from the cosine for simplicity and included a factor of $\pi/2$. As a result, this λ varies from 0 (no path information) to 1 (perfect path information). The actual coupling coefficients for the different plots are given in Figs. 4.2, 4.3, and 4.4, which were created with the following code:

```
Manipulate[
Plot[10*DSD[y/100, \[Lambda]], {y, -2, 2}, PlotRange -> Full,
Frame -> True, FrameStyle -> Directive[Black], Axes -> False,
FrameLabel -> {Style["\!\(\*SubscriptBox[\(y\), \(f\)]\)  (cm)",
Plain, 16, FontFamily -> "Times New Roman"],
Style[ToExpression["80 \\pi \\hslash d(h_{u l},h_{u l})",
TeXForm], Plain, 16, FontFamily -> "Times New Roman"]},
FrameTicksStyle -> Larger, PlotStyle -> {Black, Thick}], {\[Lambda], 0, 1}]
```

List of Figures

Bibliography

[1] David H. McIntyre, *Quantum Mechanics* (Pearson Addison-Wesley, San Francisco, California, 2012).

[2] David A. Craig and Parampreet Singh, Consistent probabilities in Wheeler-DeWitt quantum cosmology, Physical Review D **82**, 123526 (2010).

[3] George Greenstein and Arthur G. Zajonc, *The Quantum Challenge*, 2nd ed. (Jones and Bartlett, Sudbury, Massachusetts, 2006).

[4] David A. Craig, The consistent histories approach to quantum cosmology, International Journal of Modern Physics D **25** (2016).

[5] Hugh Everett, "Relative State" Formulation of Quantum Mechanics, Rev. Mod. Phys. **29**, 454–462 (1957).

[6] James B. Hartle, The impact of cosmology on quantum mechanics, arXiv **1901.03933v1 [gr-qc]** (2019).

[7] James B. Hartle, Spacetime quantum mechanics and the quantum mechanics of spacetime, arXiv **gr-qc/9304006v3**, 1–28 (2014).

[8] Robert B. Griffiths, Consistent histories and the interpretation of quantum mechanics, J. Stat. Phys. **36**, 219–272 (1984).

[9] Roland Omnès, Consistent interpretations of quantum mechanics, Rev. Mod. Phys. **64**, 339–382 (1992).

[10] H.D. Zeh, On the interpretation of measurement in quantum theory, Found. Phys. **1**, 69 (1971).

[11] W. H. Zurek, Pointer basis of quantum apparatus: Into what mixture does the wave packet collapse?, Phys. Rev. D **24**, 1516–1525 (1981).

[12] E. Joos and H.D. Zeh, The emergence of classical properties through interaction with the environment, Zeitschrift für Physik B Condensed Matter **59**, 223–243 (1985).

[13] Thomas Young, II. The Bakerian Lecture. On the theory of light and colours, Phil. Trans. R. Soc. **92**, 12–48 (1802).

[14] A. Tonomura, J. Endo, T. Matsuda, T. Kawasaki, and H. Ezawa, Demonstration of single-electron buildup of an interference pattern, American Journal of Physics **57**, 117–120 (1989).

[15] Randall D. Knight, *Physics for Scientists and Engineers: a Strategic Approach with Modern Physics*, 4th ed. (Pearson Education, Inc., 2017).

[16] Max Born, Zur Quantenmechanik der Stoßvorgänge, Zeitschrift für Physik **37**, 863–867 (1926).

[17] Claude Cohen-Tannoudji, Bernard Diu, and Franck Laloë, *Quantum Mechanics*, Vol. 1 (Hermann, Paris, France, 1977).

[18] K. A. Kirkpatrick, Translation of G. Lüders' Über die Zustandsänderung durch den Meßprozeß, arXiv **quant-ph/0403007v2** (2006).

[19] Gerhart Lüders, Über die Zustandsänderung durch den Meßprozeß, Annalen der Physik **8** (1951).

[20] Tabish Qureshi, Interference visibility and wave-particle duality in multipath interference, Phys. Rev. A **100**, 042105 (2019).

[21] Jonathan J. Halliwell, Somewhere in the universe: Where is the information stored when histories decohere?, Physical Review D **60**, 1–8 (1999).

[22] Tabish Qureshi, Coherence, interference and visibility, arXiv **1905.00917v4 [quant-ph]** (2019).

[23] Wolfram Research, Inc., Mathematica, Version 12.0 Student Edition, Champaign, IL, 2019.

[24] François Bardou, Transition between particle behavior and wave behavior, Am. J. Phys. **59** (1991).